

HYDRAULIC MODELING OF MECHANICAL
DESTRATIFICATION OF LAKES

By

NADER SHARABIANLOU
"

Bachelor of Science

Oklahoma State University

Stillwater, Oklahoma

1974

Submitted to the Faculty of the Graduate College
of the Oklahoma State University
in partial fulfillment of the requirements
for the Degree of
MASTER OF SCIENCE
December, 1975

Thesis

1975

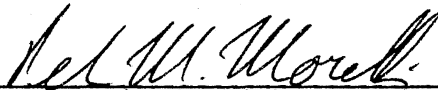
S531h

Cop. 2

MAR 24 1976

HYDRAULIC MODELING OF MECHANICAL
DESTRATIFICATION OF LAKES

Thesis Approved:



Thesis Adviser



Dean of the Graduate College

935081

ACKNOWLEDGMENTS

I would like to express my appreciation to my adviser, Dr. D. K. McLaughlin, for his patient and invaluable guidance and assistance throughout this study. The time, advice and criticism of the chairman of my committee, Dr. P. M. Moretti, is especially appreciated. Appreciation is also extended to Dr. J. D. Parker for his valuable suggestions.

I would like to thank my good friends, A. J. Smith, David Bogard and Tim Troutt, for their contributions of time and advice.

I appreciate the efforts of Eldon Hardy in the preparation of the illustrative material and Ms. Charlene Fries, who was responsible for putting this thesis in its final form.

I deeply appreciate the encouragement and moral and financial support given by my parents, Mr. and Mrs. Rahim Sharabianlou.

This project was funded by the Oklahoma Water Resources Research Institute.

TABLE OF CONTENTS

Chapter	Page
I. INTRODUCTION	1
Field Research	2
Significance of Modeling	3
Background in Lake Modeling	4
Objective	6
II. IMPORTANT DEFINITIONS AND PARAMETERS	8
Modeling Parameters	8
Criterion for Evaluating Destratification	11
Destratification Efficiency	12
III. PROTOTYPE DESTRATIFICATION	14
IV. EXPERIMENTAL APPARATUS	17
Model Basin	17
Model Pump	18
Shaft Speed Measurements	18
Velocity Measurements	19
Power Measurements	19
Data Collection	19
Density Measurements	20
Experimental Procedure	20
Data Reduction	21
V. EXPERIMENTAL RESULTS	22
Shrouded Propeller No. 1	22
Shrouded Propeller With Skirt	25
Unshrouded Propeller No. 1	26
Unshrouded Propeller No. 2	28
Comparison of the Results	29
VI. CONCLUSIONS	31
A SELECTED BIBLIOGRAPHY	32
APPENDIX A - TABLES AND FIGURES	34
APPENDIX B - CONDUCTIVITY PROBE	60

Chapter	Page
APPENDIX C - VELOCITY MEASUREMENTS	62
APPENDIX D - POWER MEASUREMENTS	64
APPENDIX E - COMPUTER PROGRAM	66

LIST OF TABLES

Table	Page
I. Parameters of Prototype and Model Lakes for Destratification Experiments	35
II. Properties of Model Experiments Matching the Prototype Richardson Number	36
III. Properties of Model Destratification Experiments for Different Configurations	37

LIST OF FIGURES

Figure	Page
1. Schematic of Ham's Lake	38
2. Schematic of the Mechanical Pump Used by Garton	39
3. Average Temperature and Density Profiles in Ham's Lake Just Preceding the Prototype Experiment	40
4. Density Profiles Recorded Throughout the Prototype Destrati- fier Experiment	41
5. Plot of the Stability Index Versus Time for the Prototype Destratification Experiment	42
6. Density Profiles Recorded Throughout the Model Destratifica- tion Experiment A.4	43
7. Comparison of Stability Index Measurements Made in the Model With Those Made in the Prototype Lake During Destratifica- tion	44
8. Comparison of Stability Index Measurements Made in the Model for Various Re	45
9. Plot of Richardson Number Versus Nondimensional Time for Model and Prototype Experiments	46
10. Progression of the Stability Index With Time for Shrouded and Skirted Propeller	47
11. Progression of Stability Index With Time for Shrouded and Unshrouded Propeller No. 1 (Richardson Number .398)	48
12. Comparison of Stability Index Measurements Made for Shrouded and Free Propeller No. 1 With Richardson Number 1.408 . . .	49
13. Plot of Shaft Input Power Versus Shaft Rotational Speed for Different Input Powers of the Motor	50
14. Calibration of Input Power to the Motor Versus Shaft Rota- tional Speed for Different Configurations	51

Figure	Page
15. Comparison of Stability Index Measurements Made for Shrouded and Unshrouded Propeller No. 1 With the Same Shaft Input Power	52
16. Visualization of the Lensing Phenomenon for the Free Propeller No. 2	53
17. Comparison of Stability Index Measurements Made for Free Propellers 1 and 2 With the Same Richardson Number	54
18. Comparison of Stability Index Measurements Made for Free Propellers 1 and 2 With the Same Shaft Input Powers	55
19. Schematic Diagram of Conductivity Probe	56
20. Sample Calibration Curve for a Conductivity Probe	57
21. Plot of Velocity Versus Shaft Rotational Speed for Different Configurations	58
22. Calibration of Torque Versus Shaft Rotational Speed	59

NOMENCLATURE

DE	destratification efficiency = $\frac{\text{net change in stability from } t_1 \text{ to } t_2}{\text{total energy input from } t_1 \text{ to } t_2} \times 100$
Fr	Froude number = $\frac{U}{(gL)^{1/2}}$
g	gravitational constant
h	height of center of gravity of the lake/model from the bottom
H	maximum depth of lake or basin
J	basic definition of overall Richardson number = $\frac{g\Delta\rho L}{\rho U^2}$
L	a characteristic length
Q	volume flow rate of pump
Re	Reynolds number = $\frac{UL}{\nu}$
Ri	Richardson number = $\frac{-g\partial\rho/\partial z}{\rho(\partial u/\partial z)^2}$
SI	nondimensional stability index = $\frac{\rho g(h_h - h)}{\rho g(h_h - h_s)}$
t	time
t _e	characteristic time of mechanical destratification = $\frac{V}{Q}$
t*	nondimensional time = $\frac{t}{t_c}$
u	local velocity in the X direction

U	characteristic velocity
V	volume of lake or model basin

Greek Letters

ν	kinematic viscosity
ρ	fluid density
ρ_t	initial density at surface of water

Subscripts

d	destratification
h	homogeneous
m	model
p	prototype
s	stratified

CHAPTER I

INTRODUCTION

Thermal stratification occurs in almost all lakes and reservoirs. In shallow impoundments the stratification may be weak. In deep lakes and reservoirs in which the storage volume is large compared to the annual throughflow, strong stratification is generally developed. The hydraulic model developed in this study is concerned with the latter situations in which the water temperature is a function of depth and time.

According to a study by Harleman et al. (1):

The primary causes of thermal stratification are the low thermal conductivity of water, the limited penetration of radiant heat and light, and the fact that stream inflows tend to be warmer than reservoir surface water. Usually all heat, apart from advected heat enters the reservoir through the surface in the form of the radiant energy. A high percentage of this energy is absorbed in the top few meters and thus the water near the surface is heated more quickly than the lower layers. This warm water tends to stay at the surface, absorbs more heat, and produces a stable condition. However, evaporation will always cool the surface causing convection currents. Surface cooling and convection will be enhanced by back radiation and conduction losses, especially at nights. Wind stresses on the water surface will cause mixing whenever neutral or unstable density gradient is set up by surface cooling. These processes of heating, cooling, and wind action lead to the development of a warm, freely circulating, turbulent upper region, called the epilimnion (p. 1).

It shields a colder, denser, relatively undisturbed region called the hypolimnion. The stratum of rapid temperature change is known as the thermocline. When these conditions exist, the reservoir is said to be stratified. Under thermally stratified conditions, with circulation to

the hypolimnion impeded by the thermocline, renewal of oxygen from the atmosphere cannot take place in the lower layers. This can lead to an anaerobic state and poor water quality. During a later overturn, the mixing of these waters with the rest of the reservoir may pollute all the water for a short period. Furthermore, release of this poor quality water may cause a deterioration of water quality downstream of the impoundment.

Field Research

Three types of attempts have been made to artificially mix density-stratified impoundments.

1. Mixing caused by releasing compressed air bubbles at depth.
2. Mixing caused by the discharge of a jet of water into the impoundment.
3. Mixing caused by the use of a submerged pumping system.

Symons et al. (2, 3) forced compressed air from diffuser stones at the bottom of the impoundment to create air-bubble plumes which induced mixing. Successful elimination of the stratification, and water quality improvement in reservoirs are reported by Knoppert et al. (4), Symons et al. (5), and Lackey (6). An attempt to find an optimum mechanical aeration system was reported by Hogan et al. (7).

The second type of technique used in attempting to mix stratified impoundments is that of the mechanical pumping system with assorted piping. It consists of pumping apparatus which simply takes water from one elevation in the impoundment and jets it out at another. Irwin et al. (8) used this technique to pump cold dense water from near the bottom to the surface of the lake.

The third type of technique was investigated by Quintero and Garton (9) and Steichen (10) using submerged axial-flow pump to move the oxygen-rich water from the surface of a lake to the oxygen-deficient water at the bottom. The application of mechanical pumping systems for mixing impoundments has been more limited than the use of compressed air systems. However, pumping systems have shown successful results in mixing process and may be designed to operate more efficiently than air systems.

Significance of Modeling

Although destratification devices of moderate size have been built by others, it has not been economically possible to try out different configurations or to optimize the design. The design parameters have largely been selected on the basis of intuition and availability. The possibility of a different more effective configuration is unknown. A large portion of the energy input is wasted and only a small percentage goes into actual mixing of fluids from different strata. In order to minimize the energy loss and the size and cost of these devices, it is important to raise the effectiveness of these components, especially if larger reservoirs are to be mixed. Since one stratification experiment on a prototype lake takes at least one summer, the advantages of a laboratory model, with the capability to run several experiments in a much shorter time are obvious. The obtained results will aid in the optimal design of destratification devices and in the sizing and selection of units for particular applications.

Background in Lake Modeling

There has been considerable amount of work done in the past few years pertinent to the topics of lake destratification and to modeling of various lake flow situations. Several mathematical models have been developed to analyze the flow situations in lakes and reservoirs. Mathematical models based upon the one-dimensional heat transfer equation for heat flux, absorption and transmission of solar radiation, and properties of circulation in stratified lakes have been developed by Dake and Harleman (11), Ryan and Harleman (1), and Lugget and Lee (12). Simulation models have also been developed to analyze the applicability of these techniques to lakes and reservoirs. An example of which is a model generated by Ditmar (13) for the prediction of changes in the density structure of an impoundment due to mixing by a pumping system.

There is active research in the general area of hydraulic modeling, some involving stratified bodies of water. One example is modeling the hydraulics and thermal dispersion in an irregular estuary by Boericke and Hall (14). An interesting example of work done on hydraulic models is the design of a new type of water channel with density stratification by Odell and Kovasznay (15).

Of particular importance of the present study is the ongoing research of Quintero and Garton (9) which involves the full scale testing of particular destratification device. Quintero and Garton (9) have reported the temperature and dissolved oxygen distributions in Ham's lake which they mechanically destratify with a large pump. The destratification experiment which is modeled in the present study is the situation in which the prototype lake is initially strongly stratified.

(This is primarily a seasonal thermal stratification.) The experiment begins with turning on of the mechanical pump which destratifies the prototype lake in from one to three weeks. This experiment is the experiment of most importance in meeting the objectives of the present study, to develop the modeling technique in stratified lake flows to the state where reliable prediction of prototype lake mixing phenomenon is possible. The model is Ham's lake constructed by Gibson (16) was the basic facility used in the present study. The major features of present model experiments are:

1. The lake is initially strongly stratified.
2. The destratification pump is a model of the one used by Steichen (10).
3. The lake model has vertical scale exaggeration.

The density differences in the prototype lake may be due to temperature differences; in the model, thermal stratification is impractical. The required temperature differences are too great, the boundary conditions of conduction from the bottom of the lake or radiation, convection, and mass transfer from the surface are not the same in the model and the prototype. However, if the fluid has similar thermal and molecular diffusivity (i.e., if the Lewis number is near 1) or if the major mechanism of mixing is turbulent rather than diffusion--both of which conditions are true in this case--density differences due to temperature may be modeled by density differences due to dissolved salts.

There are a number of salts which can increase the density of water by about 80%; common table salt can give about a 20% increase--less if the solution has to be clear--but it is convenient and inexpensive and a

few percent weight density increase is adequate for the needed experiments.

Although there is considerable experience in the literature with modeling with vertical scale exaggeration (17, 18, 19) and with stratified water ways (20), no report was found of hydraulic model studies which involve all three of the major features of present model experiment listed above. The distorted model used with the present study has a horizontal scale factor of 1 to 360 and vertical scale factor of 1 to 34. The practice of scale distortion can be subjected to much criticism. Fisher and Holley (17) have stated that distorted models should not be used to model dispersion since "a distorted hydraulic model magnifies the dispersive effects of vertical velocity gradients and diminishes the effects of transverse gradients" (p. 51). However, Keulegan (21) and Barr and Hassan (22) have reported moderately good success in modeling exchange flows in rectangular channels with distorted hydraulic models. One of the major questions of interest in the present study is what experimental data could be obtained, in direct or corrected form, which will be useful for the predictive purposes.

Objective

The major goal of the present study was to determine the relative mixing efficiencies of different pump configurations. The major objectives of the study can be broken down into three categories.

1. To determine the effect of varying propeller size on mixing efficiency.

2. To determine the effects of geometrical constraints on mixing efficiency. (I.e., does a jet with a shroud or diffuser have a higher

mixing efficiency than a free jet?)

3. To determine if results obtained from model experiments can be justifiably applied to the prototype situation.

CHAPTER II

IMPORTANT DEFINITIONS AND PARAMETERS

This chapter is intended to present the modeling parameters, such as scale factors, related nondimensional numbers, and in particular Richardson Number. The important definitions, such as stability index and destratification efficiency used throughout this text, are also presented in this chapter and their significance is discussed in detail.

Modeling Parameters

In modeling any free surface stratified hydraulic system, three nondimensional parameters are of importance. These three parameters are:

1. Froude Number:

$$Fr = \frac{U}{(gL)^{1/2}} ;$$

2. Reynolds Number:

$$Re = \frac{UL}{\nu} ;$$

3. Richardson Number:

$$Ri = \frac{-g\partial\rho/\partial z}{\rho\left(\frac{\partial u}{\partial z}\right)^2} .$$

Froude number becomes a part of the governing equation if there is an open surface, as on a lake, with a high density below it and a negligible density above it. In flow situations such as one being analyzed

in the present study, where the open surface waves are negligible and the entire surface of the lake is assumed to be at the same level, Froude number becomes an unimportant parameter. Such would not be the case if there were substantial mean current due to a throughflow in the lake. However, in the model the Froude number is large; it may, for example, reach a critical value at which the surface depression over pump inlet may be so great that air is entrained and cavitation occurs. It is necessary to limit the velocity increase and size reduction in the model to make sure that the Froude number does not become important.

The consequence of limiting Froude number is that either the models must be large (i.e., the characteristic length reduced by only a moderate ratio, and the reference velocity increased by only the same ratio); or that the Reynolds number is lower in the model than in the prototype (i.e., the reference velocity is not increased in proportion to the scaling ratio). There is considerable experience in the use of too-small Reynolds numbers in models. It is known that this deviation from strict similitude leads to only moderate errors, if the flow regimes (i.e., laminar or turbulent flow) are still the same in the model. The situation will be discussed later where there is less mixing in the model, due to the lower Reynolds number (Chapter IV).

Another possible compromise is the use of geometric distortions. For example, the horizontal scale may be chosen to be a very small ratio (1 to 360 in this case), so that the model will fit into a given facility, while the vertical scale is a bigger ratio (i.e., 1:34 in this case), so that lower Froude numbers and higher Reynolds numbers (for the boundary layer on the bottom) are possible. However, this represents a deviation from the prototype as mentioned by Fisher and Holley (17)

which cannot be analyzed in terms of similitude. As one objective of this study, experiments were attempted to examine this problem in some detail.

Richardson number is the most important nondimensional parameter in hydraulic modeling of stratified flows. This parameter relates to the terms of the governing equation which are most important to the phenomena concerned with the primary objective of this study. In the form of densimetric Froude number or its inverse, overall Richardson number is defined to be

$$J = \frac{g\Delta\rho L}{\rho U^2}$$

where $\Delta\rho$ is a reference density difference (i.e., difference in the density between the top and bottom of the lake) and L is the characteristic length, taken vertically if there is a geometric distortion.

Overall Richardson number is derived from the gradient Richardson number

$$R_i = \frac{-g\partial\rho/\partial z}{\rho(\frac{\partial u}{\partial z})^2}$$

by assuming that the density gradient $\frac{\partial\rho}{\partial z}$ scales with a characteristic density difference $-\Delta\rho$ divided by a characteristic length, L , and the velocity gradient scales with a characteristic velocity U divided by L . To match Richardson number between model and prototype, where the depth of the model is smaller but its reference velocity greater than in the prototype, the density difference in the model must be greater in order to achieve the same Richardson number.

It is important to realize that even though the model is geometrically distorted, the mixing process is undistorted. This is a resulting fact from scaling the propeller 1:34 like vertical scale, so that the

near field modeling would be undistorted. However, the supply of unmixed fluid available to the process is reduced beyond 1:34. For the purpose of obtaining time scales of mixing the overall lake, the volume of the lake divided by the volume flow rate of the propeller was chosen as a characteristic time. This relates the mixing rate to the total basin to be mixed. Observing the dispersion of dye from above and through the dam (16), bore out the following fact: the mixing took place largely in the vicinity of the destratification propeller and the mixed, intermediate density liquid flowed outward at its proper level as a "lens." From this the important assumption was developed that the limiting process is the mixing phenomenon in the zone which was modeled correctly, and that the transport phenomenon is not the limiting factor. The time in which the mixed fluid reaches the farthest part of the lake is short (and should remain short even without geometric distortion) compared to the time necessary for total mixing. Hence we conclude that the approach used in the present study, which concentrates on the mixing process and neglects the dispersion time, is appropriate for predicting the progress of destratification as an overall process.

Criterion for Evaluating Destratification

The stability of the stratification is an important phenomenon since it quantifies the amount of energy necessary to overcome an existing stratification condition. In nondimensional form the stability index is

$$SI = \frac{\rho g(h_h - h)}{\rho g(h_h - h_s)}$$

where h is the height from the bottom of the center of gravity of the

lake, ρ is the average lake density, and the subscripts h and s stand for homogeneous and fully stratified, respectively. The stability index is the gravitational potential energy of the lake referenced to the lake in its homogeneous condition and nondimensionalized with the potential energy of the fully stratified lake (with the same reference). This index is computed from the density profiles and the elevation contours of the lake which provided the volume of the lake in every increment of elevation. If profiles are taken over a period of time calculations can be made to generate stability index versus time curves. A criterion was chosen that the model was destratified when the stability index fell below 10% of its initial value. Corresponding time for this value of stability index was called t_d^* (nondimensional destratification time).

Destratification Efficiency

Calculation and comparison of the "destratification efficiency" is a useful way of comparing the mechanical performance of artificial destratification devices. A means of calculating the effectiveness of a destratification apparatus is suggested by Symons et al. (3) in the form of the destratification efficiency (DE), defined by the ratio:

$$DE = \frac{\text{Net change of stability from } t_1 \text{ to } t_2}{\text{Total energy input from } t_1 \text{ to } t_2} \times 100.$$

It is difficult to determine in generalized terms the input energy required to drive a particular pumping system. A major portion of the losses in a system are unique to the particular pumping system and its detailed design. While consideration of these details is important to the design of a particular pumping system, the purpose of this study is

to find results which will guide the general, rather than detailed, design of the system.

CHAPTER III

PROTOTYPE DESTRATIFICATION

Ham's lake, 8 kilometers west of Stillwater, was chosen as the lake to be modeled. Ham's lake was built by the Soil Conservation Service of the United States Department of Agriculture in 1964. The surface area of the lake is 40 hectares and it has a volume of 115 hectare-meters. The lake has a maximum depth of approximately 9 meters near the dam. Figure 1 shows a map of Ham's lake. Garton and his students (e.g., Steichen [10]) have continued to conduct destratification experiments each year on Ham's lake as well as on larger lakes. The researchers used a large propeller connected to a one-half horsepower motor to force the top water downward. The propeller was enclosed in a cylindrical housing and the velocity of the water leaving the propeller was measured by a screw-type current meter located beneath the propeller. Details of pumping device used to destratify this lake and its performance are described by Quintero and Garton (9). A sketch of the pumping device used is shown in Figure 2. The researchers continuously recorded the temperature and dissolved oxygen profiles at different locations during the destratification process. Toetz, Wilhm and Summerfelt (23) have analyzed the general aspects of the biological effects of artificial destratification in Ham's lake. They have continued to monitor important biological information, including fish growth, on the lakes Garton (9) has been destratifying.

On July 16, 1973, Steichen (10) began continuous operation of the destratification pump (without the conical skirt) in Ham's lake. He reported that during the mechanical destratification of a lake, temperature (and hence density) profiles taken at different locations in the lake are not substantially different. Figure 3 is a reproduction of the average temperature profile he measured on that day and density profile deduced from the temperatures. Table I lists the pertinent information about the lake and the pump for this operation. Based upon the initial density difference and using the pump average outlet velocity as the characteristic velocity, the Richardson number for this flow calculates to be $J = \frac{g(\Delta\rho/\rho)H}{U^2} = .398$. The pertinent fluid dynamic data from this experiment can be summarized in Figures 4 and 5. Figure 4 shows a record of the density profiles measured (from temperature readings) throughout the prototype destratification experiment.

Conventional analysis of this type of data includes a calculation of the progress of the stability index with time. The progress of the stability index with time during the prototype destratification experiment is plotted in Figure 5. The time variable t has been nondimensionalized with the characteristic time t_c for this phenomenon defined as the ratio of the total volume of the lake divided by the volume flow rate of the pump, i.e., $t_c = \frac{V}{Q}$ and $t^* = \frac{t}{t_c}$. A fourth order polynomial least squares regression curve fit has been made to this data and yields the curve in the figure. The portion of the curve from the prototype experiment which shows a stability index increase between the nondimensional times of 1.2 and 1.5 is due to the climatological effects. This type of effect was not modeled in the present research program. Using the 10% stability index criterion, the value of $t_d^* = .76$ ($t_d = 15.1$ days)

is obtained for the prototype experiment. This nondimensional destratification time is one of the most important parameters of the physical process which is hoped to be able to predict with the use of the hydraulic model in the present study.

CHAPTER IV

EXPERIMENTAL APPARATUS

In this chapter the experimental apparatus and procedures are described. The test facilities are essentially those used by Gibson (16) with some additions and modifications.

Model Basin

A 3785 liters basin with the model of Ham's lake inserted was the basic facility used in the present study. Plexiglass on the dam side of the basin allowed the visualization of the flow situations. This hydraulic distorted model has horizontal and vertical scale ratios of approximately 1 to 360 and 1 to 34, respectively. This gives what appears to be a reasonable balance between compactness, vertical distortion, and feasible Reynolds number. The volume of the lake is an important parameter in determining the destratification time. A portion of the total volume of the Ham's lake is included in a number of tortuous limbs. As a compromise, the limbs were modeled accurately as to depth, width, etc., but bent around so as to keep the overall dimensions down. The destratification device used is a model of the one used by Steichen (10) (see Figure 2).

Model Pump

The pumping device for the model was designed from the prototype pumping device on Ham's lake (see Figure 2) and run by a DC motor. The pump was inserted in the basin and was located at the same nondimensional horizontal and vertical coordinates as in the prototype destratification experiment. Two three-bladed propellers of different sizes were used in four different configurations. Propeller No. 1, cut from .32 cm plexiglass was 3.175 cm in diameter. The blades were twisted to make an angle of approximately 30 degrees with the plane of the propeller hub. Propeller No. 2 was approximately 2.5 cm in diameter. As a first configuration the physical situation in the prototype destratification experiment was modeled. Propeller No. 1 was placed in a simple shroud suspended from the platform where the motor was mounted. Stator vanes were placed on top of the shroud to decrease the rotation of the fluid. In a second configuration a conical skirt was suspended beneath the shroud. The conical skirt which acted as a diffuser was modeled from the skirt used in the prototype discussed by Steichen (10). The skirt was made out of cellulose acetate and connected to the shroud by silicon-rubber sealer. The edges were carefully smoothed to prevent any turbulence caused by roughness. The third configuration was a situation where the propeller No. 1 was operated as a free propeller as the shroud and the skirt were removed. The fourth configuration was propeller No. 2 (2.5 cm in diameter) mounted as a free propeller.

Shaft Speed Measurements

Rotational speed measurements were made by means of a magnetic coil and a Beckman electronic counter. The magnetic coil sensed the magnetic

field produced by a magnet strip mounted on the shaft.

Velocity Measurements

Velocity of the water leaving the propeller in each configuration was measured by photographic tracing of dyed portion of the water. Details of the velocity measurements are discussed in Appendix C.

Power Measurements

The power input to the motor was measured by a Hickok digital voltmeter and a Weston ammeter connected in series with the pump and the power supply. The product of current and voltage determined the amount of consumed power. The efficiency of the motor was calibrated by connecting it to a torque meter sensor and measuring the amount of shaft input power at different shaft rotational speeds. The details of power calibration are discussed in Appendix D.

Data Collection

One set of data was collected during each run by means of the conductivity probe. Resistivity measurements at different depths in the model lake were made by the conductivity probe. These measurements were converted to densities by using the calibration curve for the conductivity probe of Appendix B. Resistivities and time during which measurements were made were both recorded. The experiment was completed when the density of the top was within 10% of the density of the bottom.

Density Measurements

Density measurements were made using conductivity probe specially constructed from flint glass tubing and very thin platinum wire. Details of density measurements by conductivity probe are given in Appendix B.

Experimental Procedure

The first step at the beginning of each experiment with the model was to establish a density profile similar in shape to the prototype lake experiment. Density stratification was established using sodium chloride to increase the density of water by varying amounts. Density differences established in this manner simulate density differences caused by temperature differences. Depending on the exact procedure followed and the specific gravity used, different initial profiles can be obtained. The appropriate procedure needed to reproduce the desired density profile in the model was found and the resulting density versus depth curve was similar in shape to the Ham's lake curve.

The procedure consisted of filling the lake with fresh water up to a height of 21.0 cm. A solution of 1.014 specific gravity was produced in the overhead tank by dissolving pure table salt in fresh water. This solution was slowly introduced into the model at the rate of 1.9 liters/min with the garden hose located perpendicularly under the pump and approximately 1.25 cm above the bottom until the height of 23.0 cm was reached. Solutions of 1.023 and 1.030 specific gravities were produced by dissolving more salt in the overhead tank. These solutions were introduced into the lake in the same manner until the heights of 24.8 and 26.3 cm were reached. The model was allowed to settle one or two

hours after reaching the final height of .263 meters, in order to let residual currents damp out.

The conductivity probe was calibrated during the preparation of the lake and an initial density profile was measured. Stratification $\frac{\Delta\rho}{\rho}$, where $\Delta\rho$ is a reference density difference (i.e., the difference in density between the top and the bottom), was measured and the desired velocity was calculated in the following manner. The overall Richardson Number $J = \frac{g(\Delta\rho/\rho)H}{U^2}$ of the experiment was initially specified, in some cases to conform to the value used in Steichen's (10) experiment. The stratification $\frac{\Delta\rho}{\rho}$ was measured; a velocity was then chosen so that the Richardson Number combination would exactly match the chosen value for the experiment. The pump was started and the velocity was brought up to its proper value. The timer was started and profiles were recorded at selected time intervals.

Data Reduction

A computer program written by Gibson (16) was modified to perform the necessary calculation needed to plot the stability index versus time curves. The model depth was divided into ten layers. Since the total depth was .263 meters, the model was subdivided into nine divisions of 2.54 cm and one division of 3.43 cm deep. Density measurements were made at the center of each division resembling the closest approximation to the density of that particular layer. The progress of the stability index with time was plotted for each experiment. From these plots non-dimensional destratification time, which is an important parameter in proving the validity of modeling technique, was obtained.

CHAPTER V

EXPERIMENTAL RESULTS

A discussion of the results obtained from various experiments on the model of the prototype pump (Shrouded Propeller No. 1) and several modified configurations are presented in this chapter. Results obtained from each configuration are discussed in separate sections. A comparison of the results was made to determine the optimum configuration.

Shrouded Propeller No. 1

Several destratification experiments with different Richardson numbers and velocity conditions were conducted using the No. 1 propeller in a simple shroud. The output data from these experiments were collected by conductivity probes and were analyzed by determining the progression of the stability index with time. Typical density profiles recorded throughout the model destratifier experiments are shown in Figure 6. A total of seven experiments with different Richardson numbers and velocity conditions were conducted. In the most significant experiments the pump output velocity and stratification were adjusted so that the overall Richardson number $J = \frac{g\Delta\rho H}{\rho U^2}$ equaled 0.398 to match the prototype experiment (10). Considering the Richardson number matching of the model and the prototype, $\frac{\Delta\rho}{\rho}$ and U are the only parameters that can be varied to keep the Richardson number at a constant value. Stratification $\frac{\Delta\rho}{\rho}$ was fixed by duplicating the initial condition from

the prototype. The value of the model velocity U was adjusted and fixed to match the Richardson number of the prototype data. Progression of the stability index with nondimensional time was plotted for the model from the measurements. Figure 7 shows this plot with the prototype experiment data superimposed on it. A fourth order polynomial least squared regression curve was fitted for both sets of data. Using the 10% stability index criterion, a nondimensional destratification time of $t_d^* = 0.88$ was obtained for the model experiment. This result is within 15% of the destratification time $t_d^* = .77$ for the prototype. The agreement was actually more successful than expected since the ratio of characteristic times of the prototype to the model was over 2000 and the Reynolds numbers ratio by a factor of 62.

Due to the high velocity operation of the pump during the destratification process for this experiment, the model lake was destratified quickly and time resolution was not as good as some other experiments conducted with different Richardson number conditions. As mentioned earlier in Richardson number matching process, the variation of one of the parameters $\frac{\Delta\rho}{\rho}$ or U causes variation of the other. A series of four experiments were conducted matching the prototype Richardson number. Different stratification conditions were produced for each of these experiments so that four different pump output velocities were used. The results obtained from these experiments are plotted in Figure 8.

Table II lists the important properties of these four experiments which matched the prototype Richardson number. It is generally believed that in the turbulent flow regime most commonly found in lake flows, the characteristics of the fluid motion are not strongly dependent on Reynolds number, provided the Reynolds number of the model is large

enough to preserve the turbulent flow. An attempt was made to analyze this problem in some detail. The four experiments conducted had varying range of Reynolds numbers. The variation of the Reynolds number in each case was made possible by adjusting the destratification and velocity conditions to the values listed in Table II.

Figure 8 shows the progress of stability index with time for these experiments. Comparison of the nondimensional destratification times obtained from this figure (listed in Table II) indicates that at moderately high model Reynolds number, where the model and the prototype Reynolds numbers differ by approximately an order of magnitude, close agreement between the model and the prototype results exists. However, at lower Reynolds numbers deviation from this agreement was indicated. Results obtained from experiments listed under A-5 and A-7 of Table II, where two experiments were conducted at almost identical Reynolds numbers, indicated the repeatability and dependability of the experiments. Results listed in Table II indicate that better mixing is a result of higher rate of the pump operation. Considering the Reynolds number effect on the validity of the modeling technique, it is apparent that increasing the model Reynolds number and bringing it closer to the prototype Reynolds number results in better modeling and closer agreement between the model and the prototype. Since the Reynolds number of the model was smaller than that of the prototype, there is probably some decrease in turbulent mixing, and the model does not replicate the destratification phenomenon. This deviation is lessened by increasing the pump output velocity and therefore increasing the model Reynolds number.

Important properties of all the experiments conducted with No. 1 propeller in a shroud are listed in Table III (experiments A-1 through

A-7) along with the experiments from the other configurations. Values of t_d^* obtained from these experiments for different Richardson numbers were recorded. Plot of Richardson number versus nondimensional destratification time was made in Figure 9.

Another interesting fact is revealed by comparing the density profiles which were measured in the model and the prototype during the destratification process, Figures 4 and 6. Most model density profiles taken during destratification had a stairstep shape characteristic of the lens of intermediate density moving through the lake. The stairstep shape of the density profiles is not as readily apparent in the prototype lake. There are probably several reasons that explain this phenomenon. First, since the Reynolds number of the model is much smaller than the prototype, there is probably some decrease in the turbulent mixing of the lens flow. There are also complicated climatological effects such as sun radiation, surface evaporation and heat transfer, surface wave induced mixing caused by wind or rainfall that increase the amount of mixing and diffusion of the mass and energy in the lake. It is expected that the model under study can replicate only the most important mixing phenomenon, namely the convection set up by the mechanical pump.

Shrouded Propeller With Skirt

Assembling a conical skirt beneath the shroud resulted in the second configuration. The conical skirt was 14.5 cm long and had a base diameter of 6.35 cm. Only one destratification experiment, where the model Richardson number was matched to its prototype value, was conducted in this case. Properties of this experiment are listed in Table III under experiment A-8. Progression of the stability index with time for this

experiment and a similar condition from the simple shrouded case are plotted in Figure 10. Nondimensional destratification times of 1.74 and 1.53 are obtained for conical skirt and shrouded case, respectively. Comparing these two results, it is apparent that operation of a pump with an installed diffuser will result in a longer period of mixing than a pump with simple shroud. However, less power input to the motor was required to drive the system when the skirt was installed. Comparing the destratification efficiencies from Table III, values of .026% and .022% were obtained for the conical skirt and simple shrouded case, respectively. This indicates that pumping systems operating with diffusers may have higher efficiencies than those operating with a simple shroud.

Unshrouded Propeller No. 1

The shroud and the conical skirt were removed and the propeller No. 1 was connected to the shaft. An attempt was made to conduct an experiment that matched the prototype Richardson number condition. The results obtained from such an experiment would be helpful in analyzing the Richardson number effect on different configurations. The prototype Richardson number was matched by adjusting the condition to those listed in Table III under experiment B-1. The progression of the stability index versus nondimensional time for this experiment and an experiment from the simple shrouded case, which was conducted at an almost identical Reynolds number, is presented in Figure 11.

From Figure 11 nondimensional destratification time of $t_d^* = .465$ is obtained for the free propeller case which compares with t_d^* of 1.53 obtained from the shrouded case. Since both of these experiments were

conducted at an identical Richardson number condition, it is apparent that operation of a pump without a shroud results in a much faster mixing time. In order to gain some insight and prove the validity of this phenomenon, the following experiment was conducted. A destratification experiment with a highly stable stratification condition (high Richardson number) from the shrouded configuration was chosen. The Richardson number and the stratification conditions were matched by adjusting the pump velocity. The progress of the stability index with time was plotted for both cases, Figure 12. A highly stable stratification condition was chosen to increase the mixing time scale compared to the measurements time so that reasonable resolution time was obtained. Nondimensional destratification times of 2.245 and 4.76 were obtained for unshrouded and shrouded cases, respectively. These results are in agreement with the ones discussed earlier in this section.

Considering the power requirements for driving a pumping system, it was apparent that less power was consumed in driving a shrouded propeller than an unshrouded one. An attempt was made to run an experiment where the power input to the shaft for both the shrouded and unshrouded configuration was equal. An experiment from the shrouded configuration with the Richardson number matching the prototype was chosen. From the power input versus rotational speed calibration curve (Figure 13), the power input during this experiment was found to be 3.30 watts. After duplicating the same stratification conditions, a trial and error technique was required to find out the power input to the motor and its corresponding shaft rotational speed which will yield a shaft input power of 3.3 watts. This was simply done by inspection from Figure 13 and referring to Figure 14 (plot of power input to the motor versus

shaft rotational speed). The velocity and the Richardson number were adjusted to the values listed in Table III under experiment B-3 to yield a shaft input power of 3.3 watts. After conducting this experiment, the progress of stability index versus time for both cases were plotted (Figure 15). Destratification times of 15.44 and 12.4 minutes were obtained for the unshrouded and shrouded cases, respectively.

This indicates that operation of a pump with a shrouded propeller will destratify a reservoir quicker than an unshrouded one for the same power consumption rate. Destratification efficiencies of .081% and .069% obtained for shrouded and unshrouded propellers, respectively, indicated the higher efficiency of the shrouded propeller.

Unshrouded Propeller No. 2

Propeller No. 1 was removed and replaced by Propeller No. 2. To analyze the Richardson number effect on different propeller sizes, a stratification and Richardson number conditions from configuration No. 3 were duplicated. (Figure 16 shows the visualization of the lensing phenomenon for this experiment.) Theoretically from the definition of the overall Richardson number $J = \frac{g\Delta\rho H}{\rho U^2}$, velocities of the same magnitude should be expected for both cases. However, as discussed earlier, the exact duplication of stratification conditions are difficult to generate. This introduces a small increase in the velocity (.222 meters/sec compared to .219 meters/sec). The progression of stability index with nondimensional time for this experiment and the experiment from configuration No. 3 case are plotted and shown in Figure 17. Nondimensional destratification times of 2.24 and 5.8 are obtained for No. 1 and No. 2 propellers, respectively. Destratification efficiency of .0034 was obtained for propeller No. 2. Comparison of this value with

destratification efficiency of .026 obtained for unshrouded propeller No. 1 indicates that operation of a pump with the unshrouded propeller No. 1 results in a higher destratification efficiency than unshrouded propeller No. 2, where both pumps operate under the same initial and Richardson number conditions.

Since propeller No. 2 required less power input to drive the system at the same rotational speed as propeller No. 1, an attempt was made to run an experiment with identical power requirements. Trial and error technique and Figures 13 and 14 were used. Conditions were adjusted to those listed in Table III under experiment C-1. The progression of stability index versus time for both propellers consuming the same power was plotted in Figure 18. Destratification times obtained (15.44 and 322 minutes for propellers 1 and 2, respectively) proved that faster mixing time will be obtained when larger propeller is used. Comparison of the destratification efficiencies obtained for both cases also proves the fact that operation of a pump with an unshrouded larger propeller is more efficient than the same system with a smaller propeller, provided both pumps consume the same power to drive the system.

Comparison of the Results

Comparison of the results obtained from different configurations indicates the following: destratification experiments conducted with the shrouded propeller with a skirt resulted in a longer period of destratification time than the simple shrouded case. Operating under the same initial and Richardson number conditions, free propeller No. 1 resulted in a much faster destratification time than propeller No. 1 with a simple shroud. Furthermore, the shrouded propeller had a lower

destratification time t_d and higher destratification efficiency DE than unshrouded propeller No. 1 when operating at the same input power.

Considering the effect of propeller size in destratification phenomenon, free propeller No. 1, operating under the same initial and Richardson number conditions as propeller No. 2, resulted in a much faster destratification time and had a much higher destratification efficiency. This was also true when both propellers operated under a condition of equal power consumption rate.

CHAPTER VI

CONCLUSIONS

The conclusions from this experimental investigation may be listed as follows:

1. Accurate prediction of the prototype destratification experiments can be achieved by means of vertically exaggerated models, using the vertical scale for modeling the destratification device.
2. The appropriate nondimensional parameters are the overall Richardson number $J = \frac{g\Delta\rho H}{U^2}$, and a characteristic time obtained from the volume of the lake divided by the volume discharge rate of the pump.
3. Operation of a pump with a shrouded propeller will result in a higher destratification efficiency than a pump with an unshrouded propeller, when both pumps have the same power consumption rate.
4. The efficiency of a pumping system operating with larger unshrouded propeller is higher than a pumping system operating with a smaller unshrouded propeller and consuming the same amount of power.

A SELECTED BIBLIOGRAPHY

- (1) Harleman, D. R. F. and P. J. Ryan. "Temperature Prediction in Stratified Water." M.I.T. Civil Engineering Department Technical Report No. 16130 DJH. Cambridge, Mass.: U. S. Environmental Protection Agency, April, 1971.
- (2) Symons, J. M., W. H. Irwin, and G. G. Robeck. "Important Water Quality Changes Caused by Mixing." J. San. Eng. Div., ASCE, Vol. 96, No. SA2 (April, 1967), pp. 1-13.
- (3) Symons, J. M., W. H. Irwin, E. L. Robison, and G. G. Robeck. "Impoundment Destratification for Raw Water Quality Control Using Either Mechanical or Diffused-Air-Pumping." J. Amer. Water Works Assoc., Vol. 59, No. 10 (October, 1967), pp. 1268-1291.
- (4) Knoppert, P. L., J. J. Rook, T. J. Hofker, and G. Oskam. "Destratification Experiments at Rotterdam." J. Amer. Water Works Assoc., Vol. 62, Pt. 2 (1970), pp. 448-454.
- (5) Symons, J. M., W. H. Irwin, R. M. Clark, and G. G. Robeck. "Management and Measurement of DO in Impoundments." J. San. Eng. Div., ASCE, Vol. 96, No. SA6 (December, 1967), pp. 181-200.
- (6) Lackey, R. T. "A Technique for Eliminating Thermal Stratification in Lakes." J. Amer. Water Resources Assoc., Vol. 8, No. 1 (February, 1972), pp. 46-49.
- (7) Hogan, W. T., F. E. Reed, and A. W. Starbird. "Optimum Mechanical Aeration Systems for Rivers and Ponds." Report No. 16080 D00. Littleton, Mass.: Littleton Research and Engineering Corp., November, 1970.
- (8) Irwin, W. H., J. M. Symons, and G. G. Robeck. "Impoundment Destratification by Mechanical Pumping." J. San. Eng. Div., ASCE, Vol. 92, No. SA6 (December, 1966), pp. 21-40.
- (9) Quintero, J. E. and J. E. Garton. "A Low Energy Lake Destratifier." Paper No. 72-599. Chicago, Ill.: American Soc. of Agr. Eng., December, 1972.
- (10) Steichen, J. M. "The Effect of Lake Destratification on Water Quality Parameters." (Ph.D. thesis, Oklahoma State University, July, 1976.)

- (11) Dake, J. M. and D. R. F. Harleman. "Thermal Stratification in Lakes: Analytical and Laboratory Studies." J. Amer. Water Works Assoc., Vol. 5, No. 2 (April, 1969), pp. 484-495.
- (12) Liggett, J. A. and K. K. Lee. "Properties of Circulation in Stratified Lakes." J. Hydraulics Div., ASCE, Vol. 97, No. H41 (January, 1971), pp. 15-29.
- (13) Ditmans, J. D. "Mixing of Density Stratified Impoundments with Buoyant Jets." W. M. Keck Lab. of Hydraulics and Water Resources, Report No. KH-R-22. Pasadena, Calif.: California Institute of Technology, September, 1970.
- (14) Boericke, R. R. and D. W. Hall. "Hydraulics and Thermal Dispersion in an Irregular Estuary." J. Hydraulics Div., ASCE, Vol. 100, No. H41 (January, 1974), pp. 85-102.
- (15) Odell, G. M. and S. G. Kovasquay. "A New Type of Water Channel with Density Stratification." J. Fluid Mechanics, Vol. 50, Pt. 3 (March, 1971), pp. 535-543.
- (16) Gibson, T. A. "Investigation of Artificial Lake Destratification --A Hydraulic Model Study." (M. S. thesis, Oklahoma State University, July, 1974.)
- (17) Fischer, M. B. and E. R. Holley. "Analysis of the Use of Distorted Hydraulic Models for Dispersion Studies." Water Resources Research, Vol. 7, No. 1 (February, 1971), pp. 46-51.
- (18) Francis, J. R. D. "Scaling of River and Estuary Models." The Engineer (London), Vol. 190 (September, 1960), pp. 329-331.
- (19) Shian, J. C. and R. R. Rumer. "Adjustment of Friction in Hydraulic Models of Lakes." J. Hydraulics Div., ASCE, Vol. 99, No. H412 (December, 1973), pp. 2251-2262.
- (20) Barr, D. I. H. "Model Simulation of Vertical Mixing in Stratified Flowing Water." The Engineer (London), Vol. 215 (January, 1963), pp. 345-352.
- (21) Keulegan, G. H. "The Mechanism of an Arrested Saline Wedge." Estuary and Coastline Hydrodynamics. New York: McGraw-Hill Book Co., 1966, pp. 56-75.
- (22) Barr, D. I. H. and A. M. M. Hassan. "Densimetric Exchange Flow in Rectangular Channels." La Houille Blanche, Vol. 18, No. 7 (November, 1963), pp. 757-766.
- (23) Toetz, D., J. Wilhm, and R. Summerfelt. "Biological Effects of Artificial Destratification and Aeration in Lakes and Reservoirs--Analysis and Bibliography." Bureau of Reclamation Report REC-ERC-72-33. Denver, Colo.: U. S. Department of Interior, 1972.

APPENDIX A

TABLES AND FIGURES

TABLE I
PARAMETERS OF PROTOTYPE AND MODEL LAKES
FOR DESTRATIFICATION EXPERIMENTS

Parameters	Prototype Experiment	Model Experiment A-4	Units
Lake volume V	1.15×10^6	.348	meters ³
Maximum depth H	9.0	.263	meters
Stratification, $\frac{\Delta\rho}{\rho}$.0025	.026	
Shroud diameter	107	3.76	centimeters
Pump flow rate, Q	0.67	4.5×10^{-4}	meters ³ /sec
Average pump outlet velo- city, U	0.74	0.41	meters/sec
Richardson number, J	0.40	0.40	
Characteristic time, t_c	1.72×10^6	767	sec
Reynolds number, $Re = \frac{UH}{\nu}$	6.56×10^6	1.06×10^5	

TABLE II
PROPERTIES OF MODEL EXPERIMENTS MATCHING THE
PROTOTYPE RICHARDSON NUMBER

Experiment	$(Re)_m = \frac{UH}{\nu}$	$(Re)_\rho = \frac{UH}{\nu}$	$J = \frac{g(\Delta\rho/\rho)H}{U^2}$	$\frac{\Delta\rho}{\rho}$	U(Meters/ sec)	t_d^*
A-4	1.057×10^5	6.56×10^6	.398	.0026	.409	.88
A-5	6.312×10^4	6.56×10^6	.398	.0092	.244	1.53
A-6	8.565×10^4	6.56×10^6	.398	.0169	.331	.95
A-7	6.382×10^4	6.56×10^6	.398	.0094	.247	1.48

TABLE III
PROPERTIES OF MODEL DESTRATIFICATION EXPERIMENTS
FOR DIFFERENT CONFIGURATIONS

Experiment	$J = \frac{g(\Delta\rho/\rho)H}{U^2}$	U(Meters/ sec)	t_d (min)	Δ (P.E.) KW-HR	Motor Input Power (Watts)	Shaft Input Power (Watts)	D.E. %
A-1	.643	.308	49.5	5.7×10^{-7}	8.20	2.40	.029
A-2	2.494	.162	432	5.74×10^{-7}	5.98	.85	.0094
A-3	1.408	.232	108.3	7.1×10^{-7}	7.20	1.75	.022
A-4	.398	.409	12.4	5.5×10^{-7}	9.20	3.30	.081
A-5	.398	.244	32.75	2.2×10^{-7}	7.35	1.94	.020
A-6	.398	.331	15	3.8×10^{-7}	8.40	2.65	.057
A-7	.398	.247	31.33	2.24×10^{-7}	7.40	1.98	.022
A-8*	.398	.253	35.95	2.3×10^{-7}	6.264	1.50	.026
B-1	.398	.265	12.88	2.5×10^{-7}	8.00	2.30	.050
B-2	1.408	.219	75	5.9×10^{-7}	7.30	1.80	.026
B-3	.602	.314	15.44	5.9×10^{-7}	9.11	3.30	.069
C-1	1.40	.222	322	6.0×10^{-7}	9.20	3.30	.0034

A - Shrouded propeller No. 1.

B - Unshrouded propeller No. 1.

C - Unshrouded propeller No. 2.

*Shrouded with skirt.

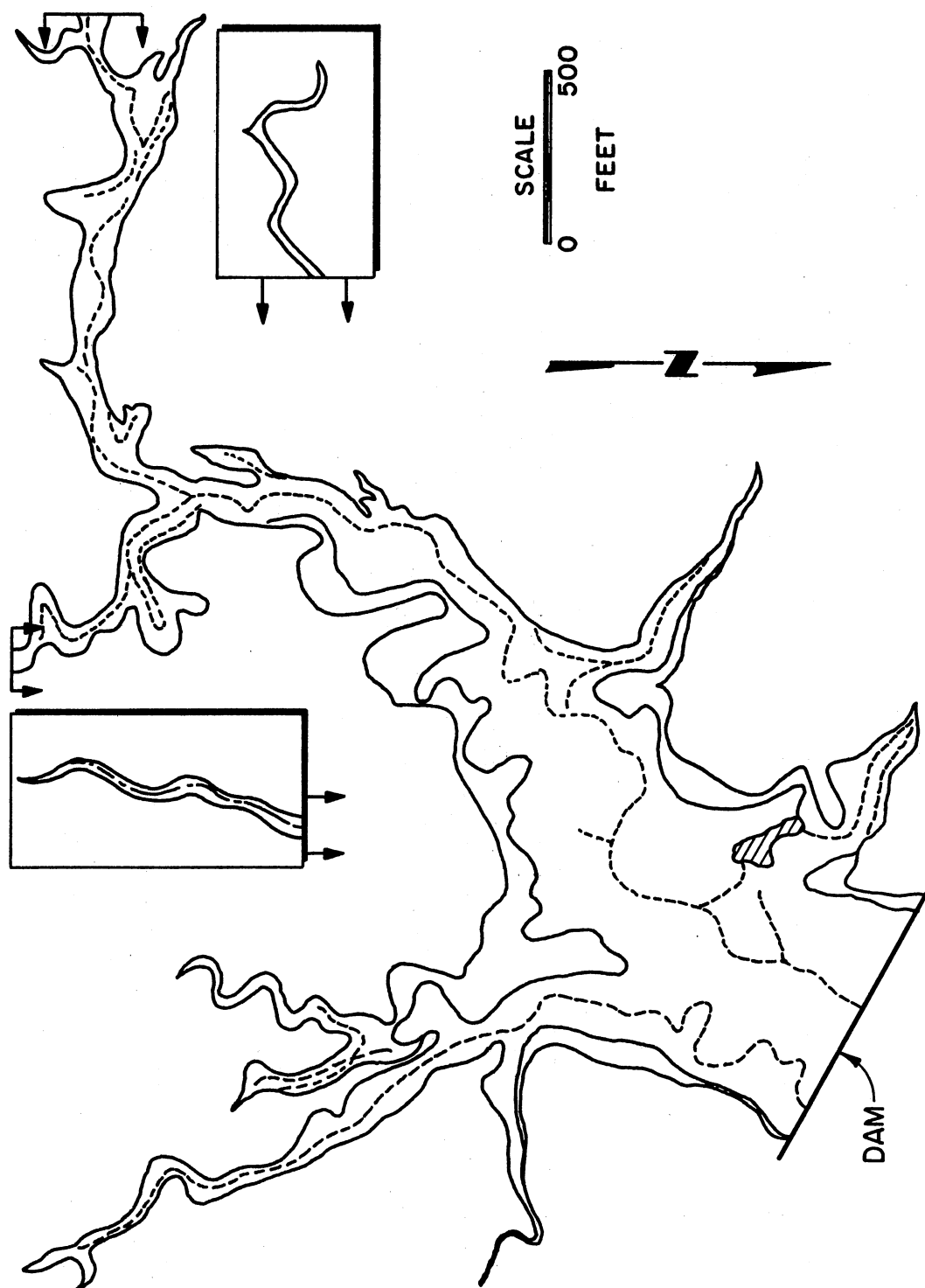


Figure 1. Schematic of Ham's Lake

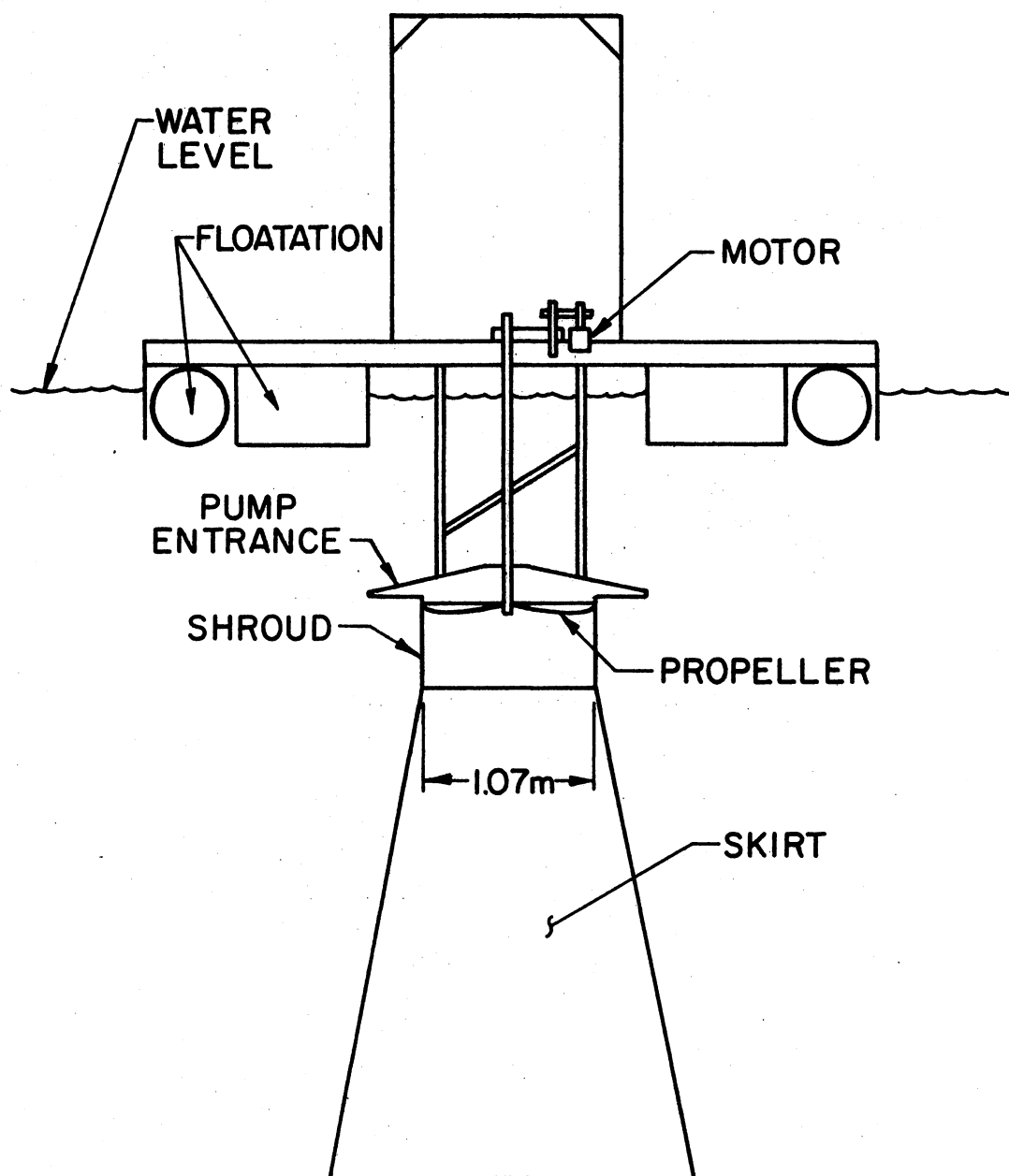


Figure 2. Schematic of the Mechanical Pump Used by Garton

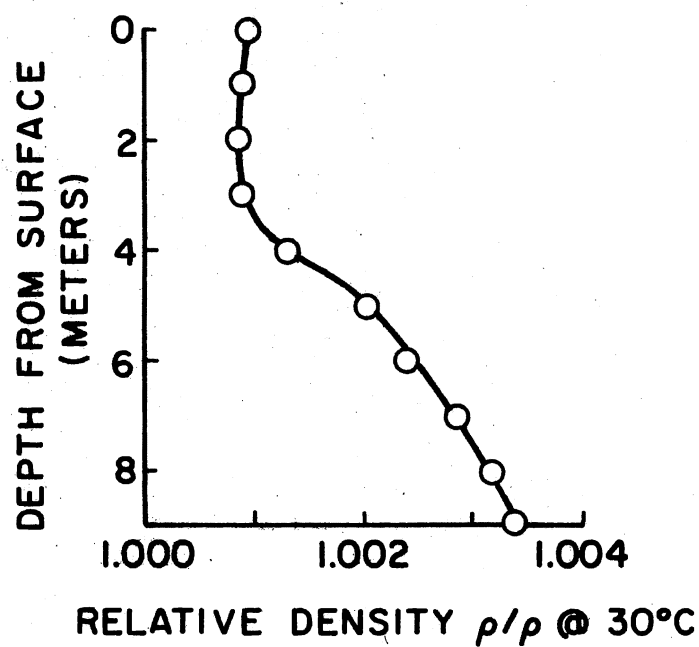
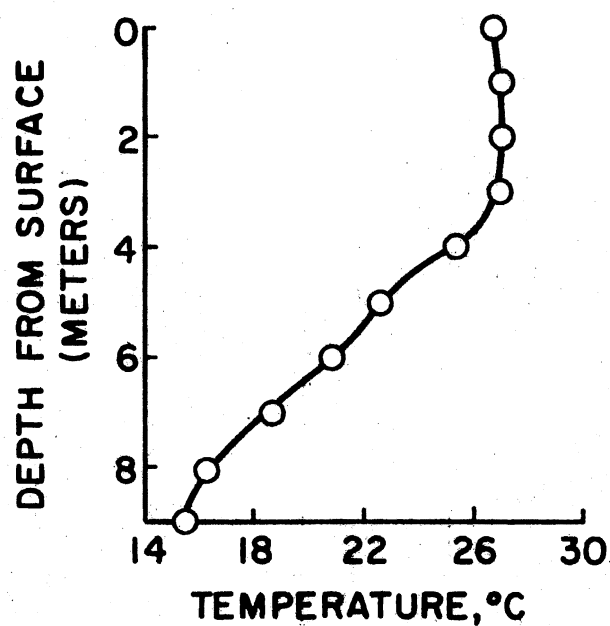


Figure 3. Average Temperature and Density Profiles in Ham's Lake Just Preceding the Prototype Experiment

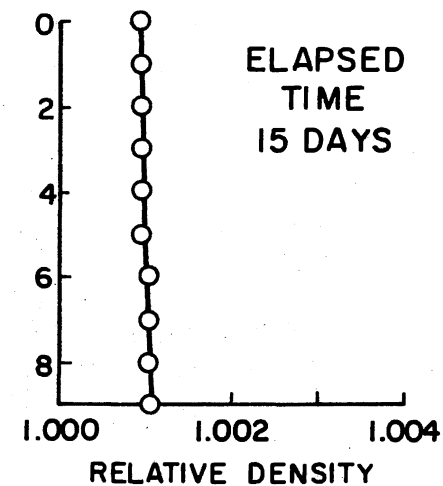
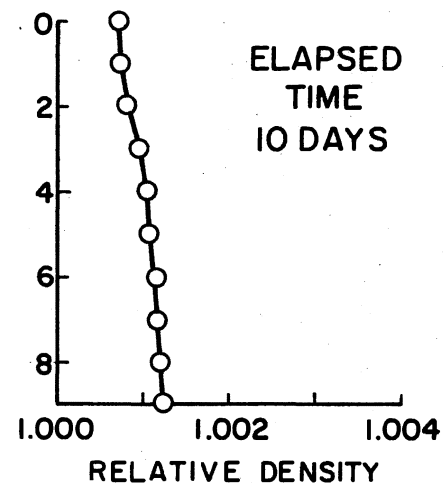
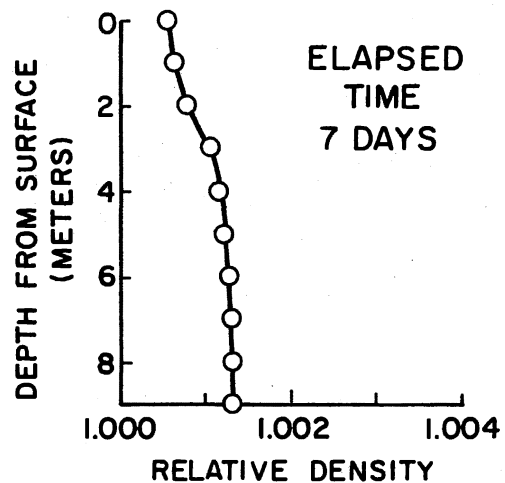
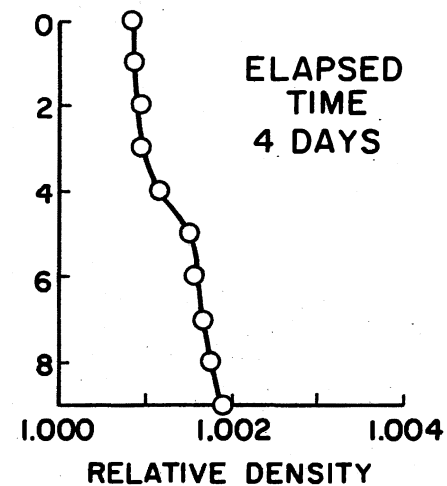
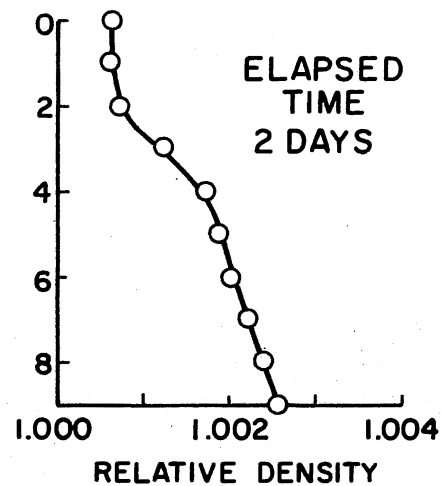
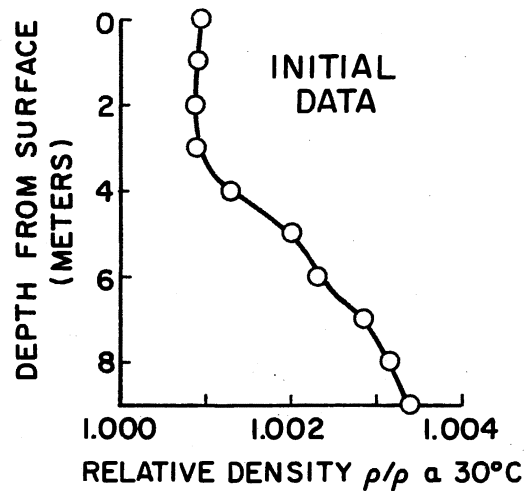


Figure 4. Density Profiles Recorded Throughout the Prototype Destratifier Experiment

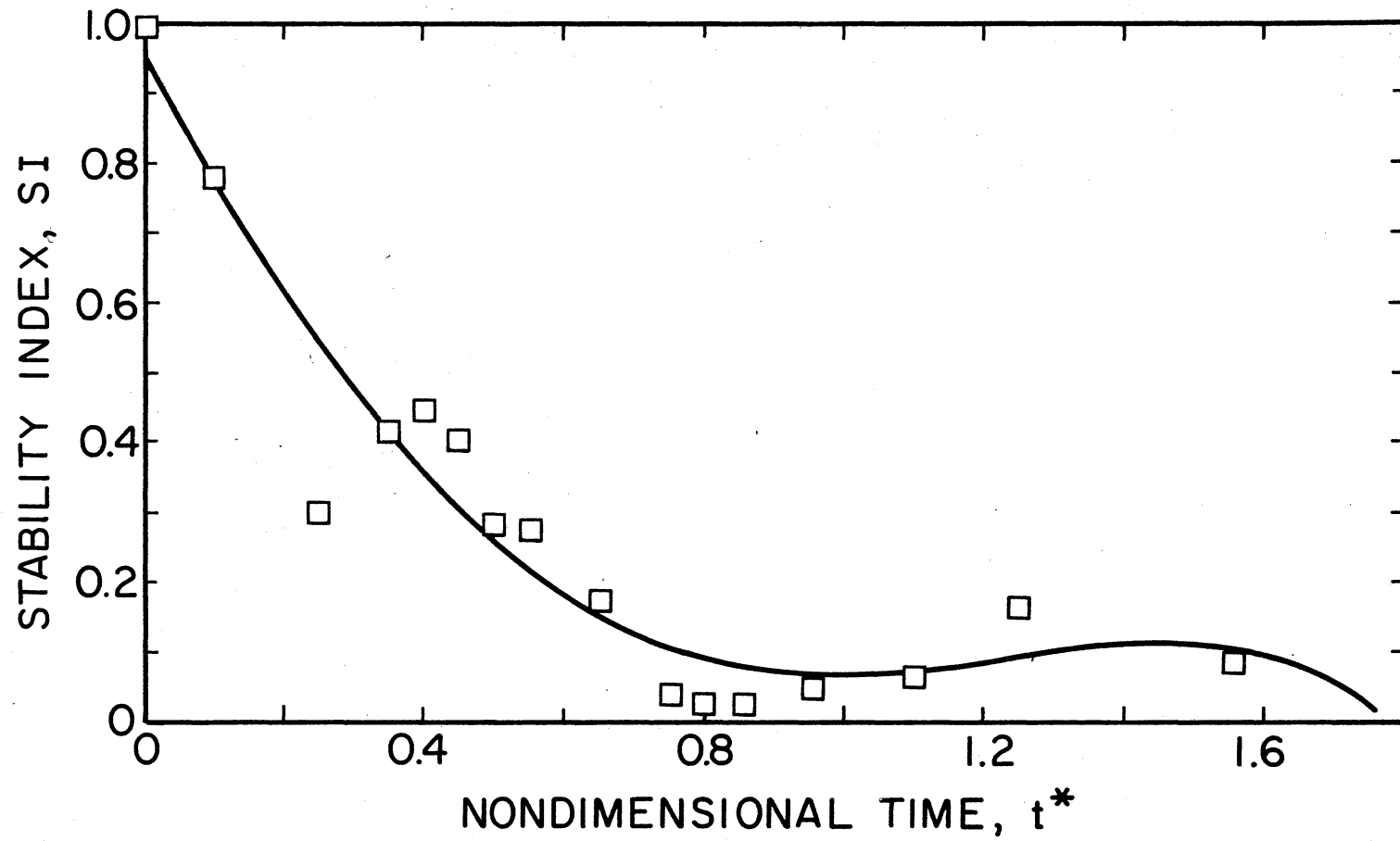


Figure 5. Plot of the Stability Index Versus Time for the Prototype Destratification Experiment

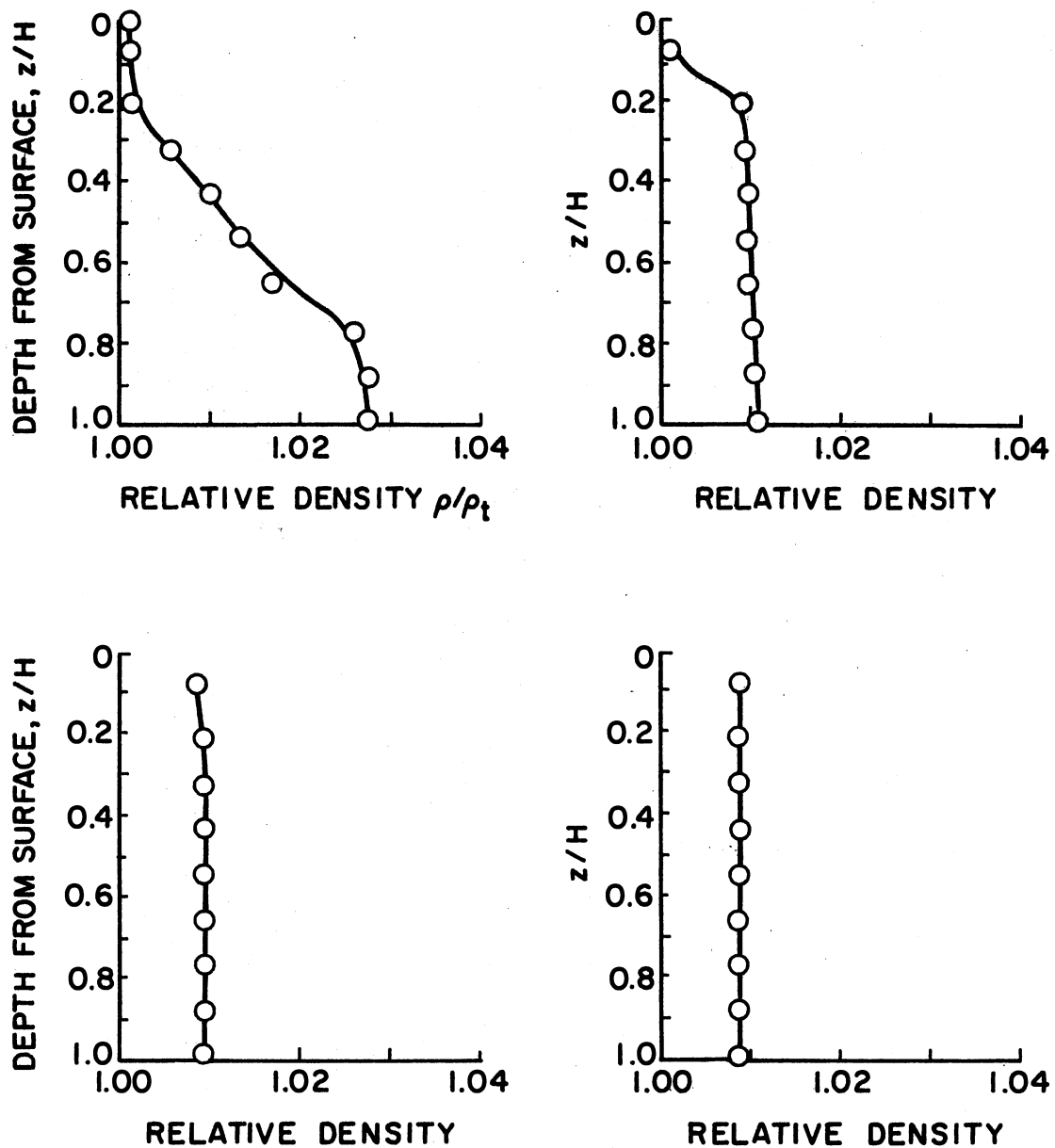


Figure 6. Density Profiles Recorded Throughout the Model
Destratification Experiment A.4

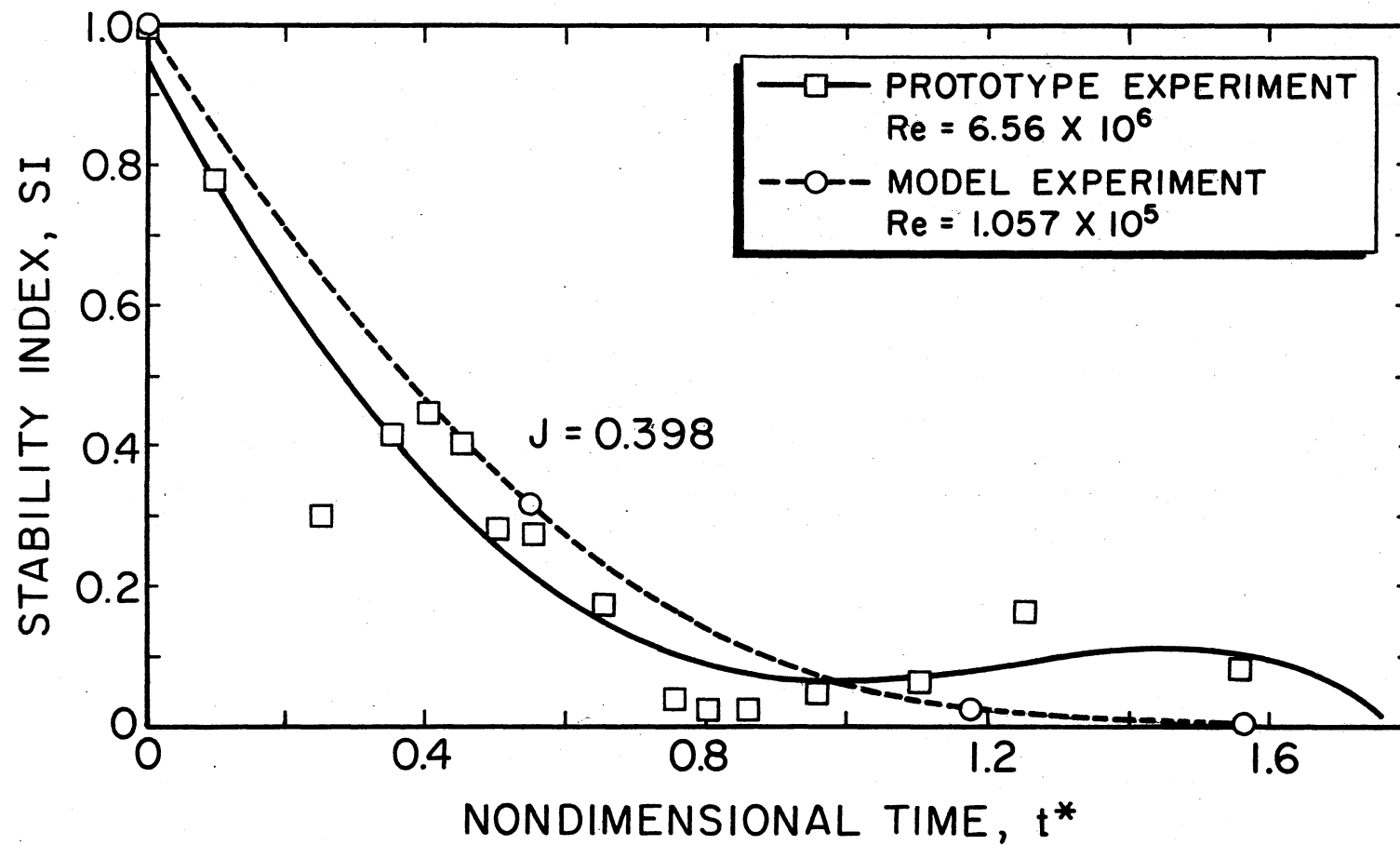


Figure 7. Comparison of Stability Index Measurements Made in the Model With Those Made in the Prototype Lake During Destratification

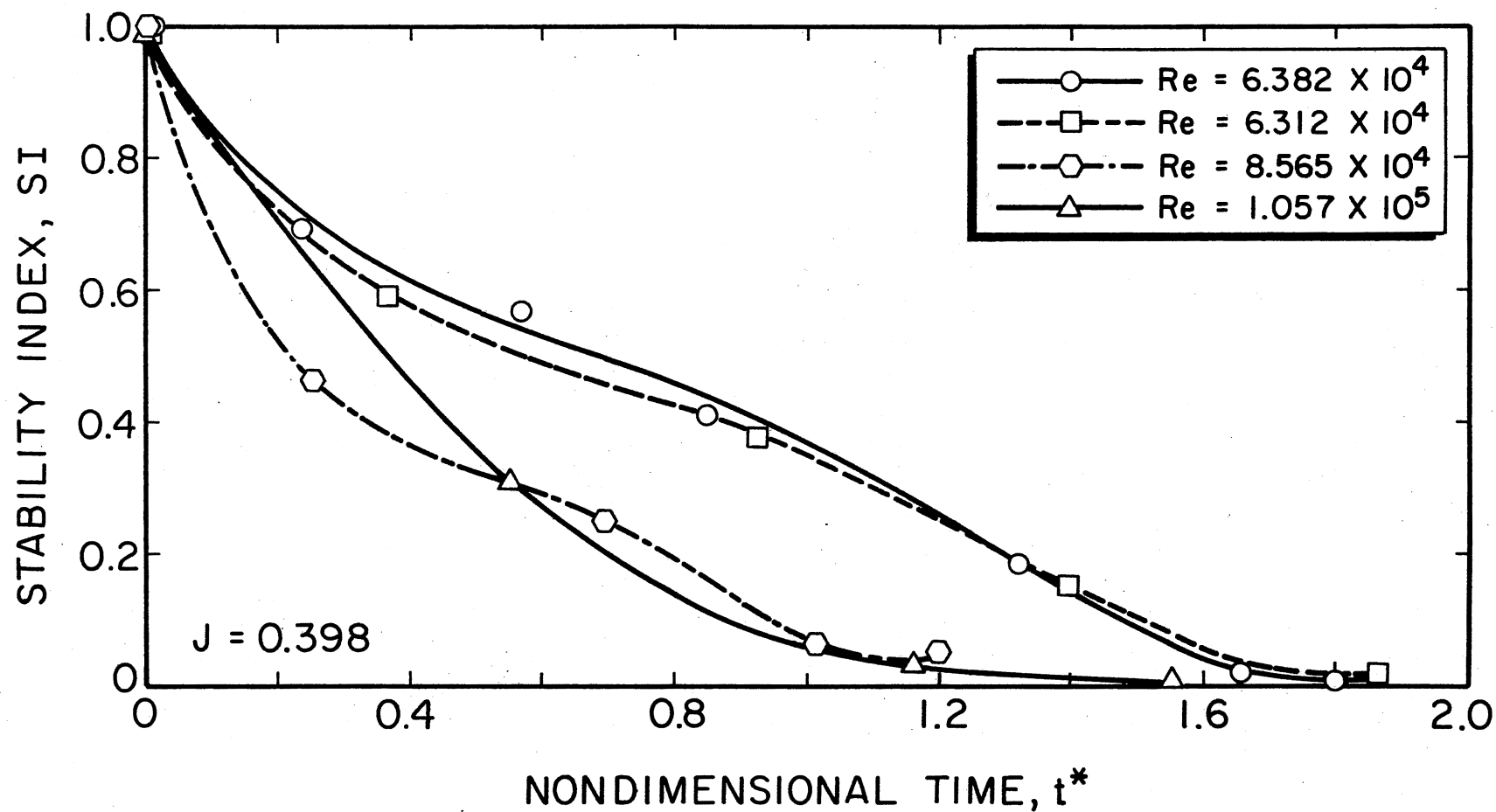


Figure 8. Comparison of Stability Index Measurements Made in the Model for Various Re

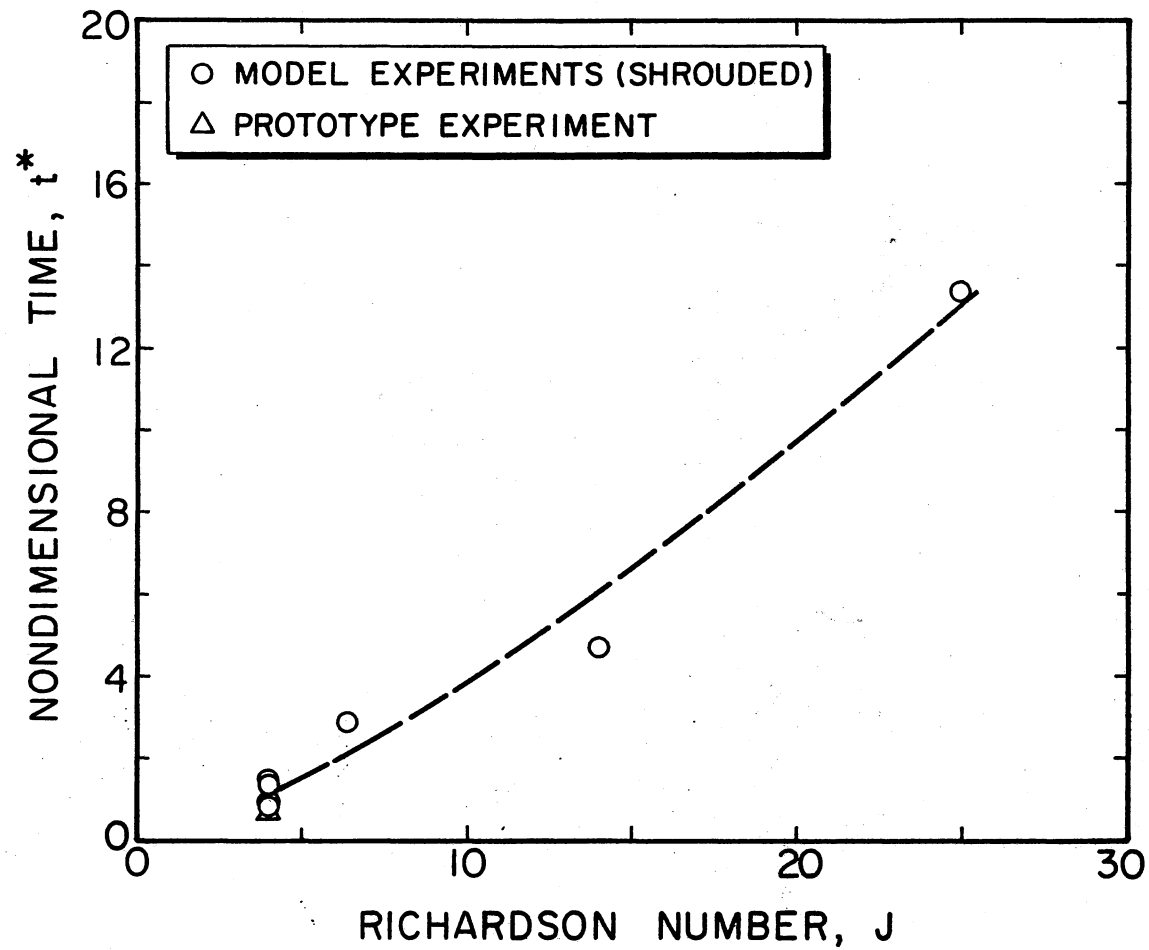


Figure 9. Plot of Richardson Number Versus Nondimensional Time for Model and Prototype Experiments

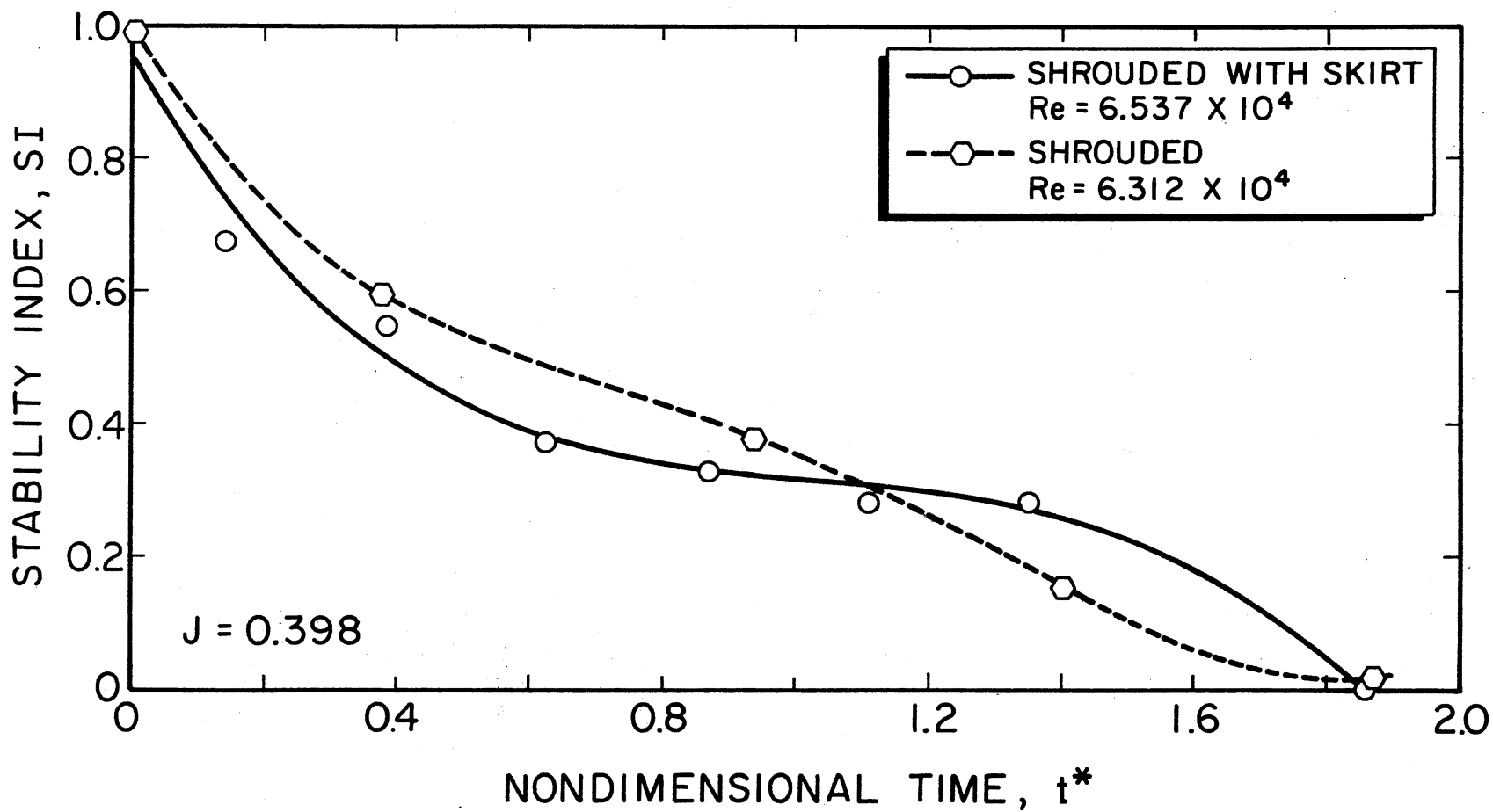


Figure 10. Progression of the Stability Index With Time for Shrouded and Skirted Propeller

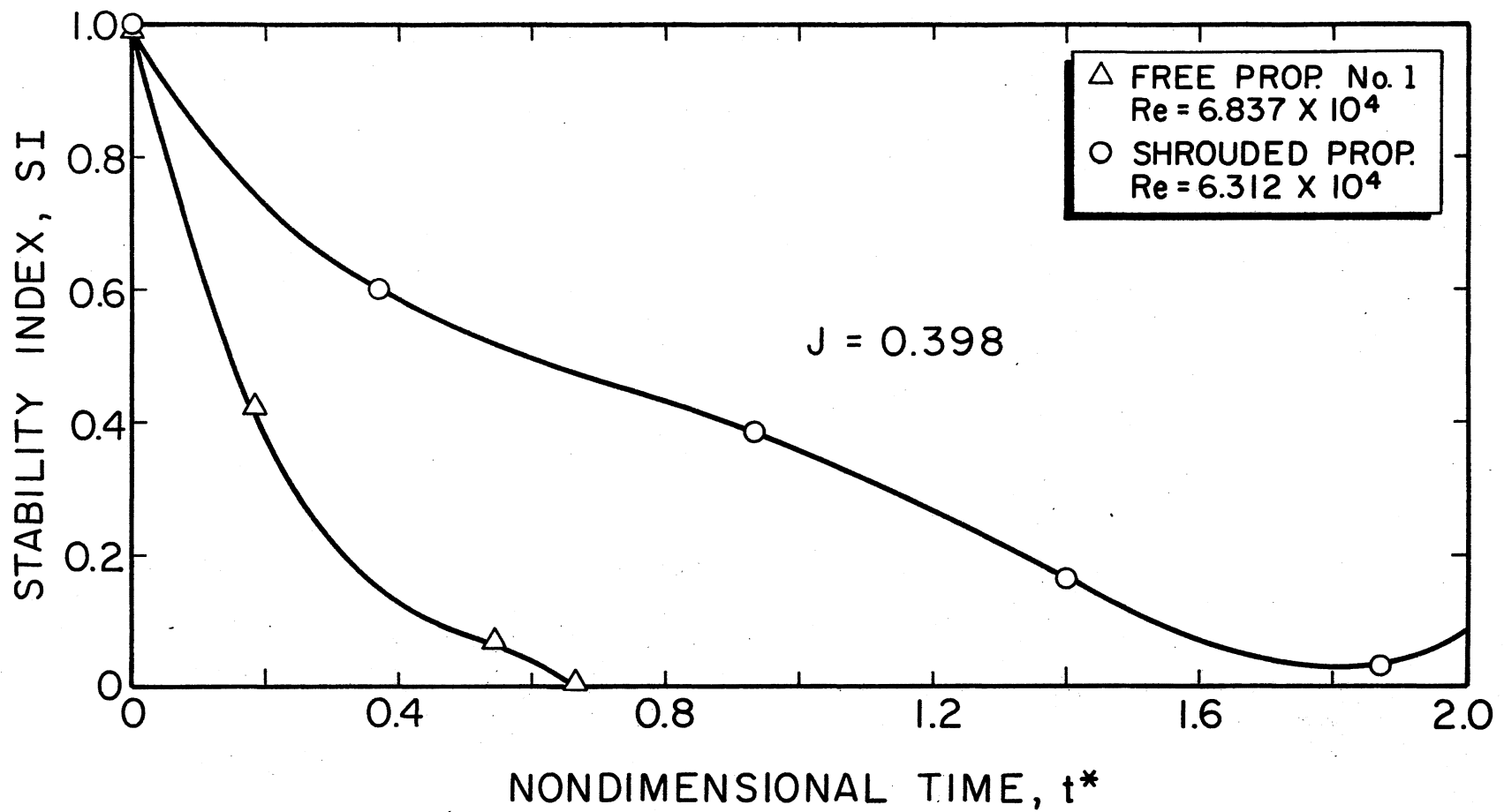


Figure 11. Progression of Stability Index With Time for Shrouded and Unshrouded Propeller No. 1
(Richardson Number .398)

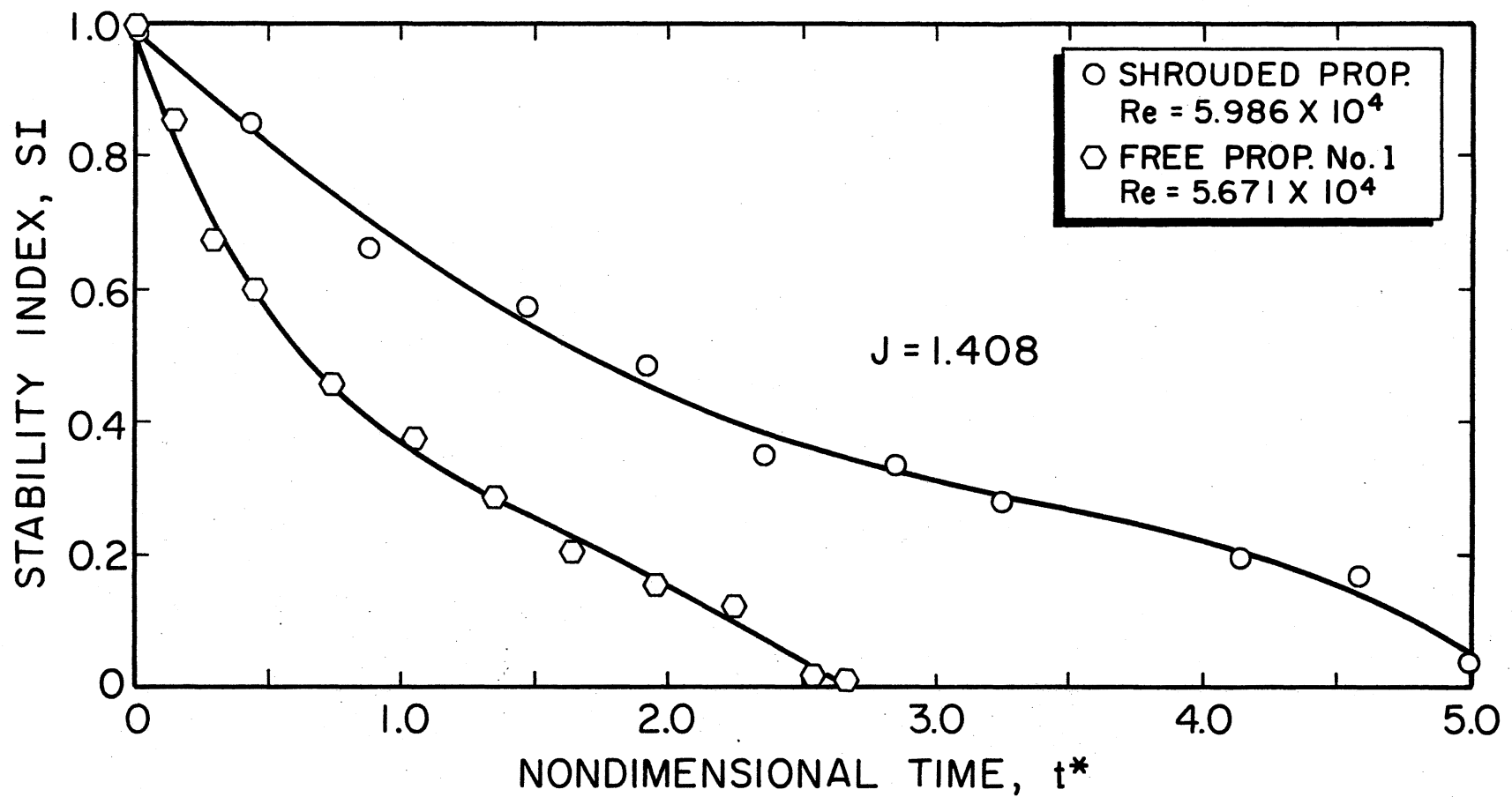


Figure 12. Comparison of Stability Index Measurements Made for Shrouded and Free Propeller No. 1 With Richardson Number 1.408

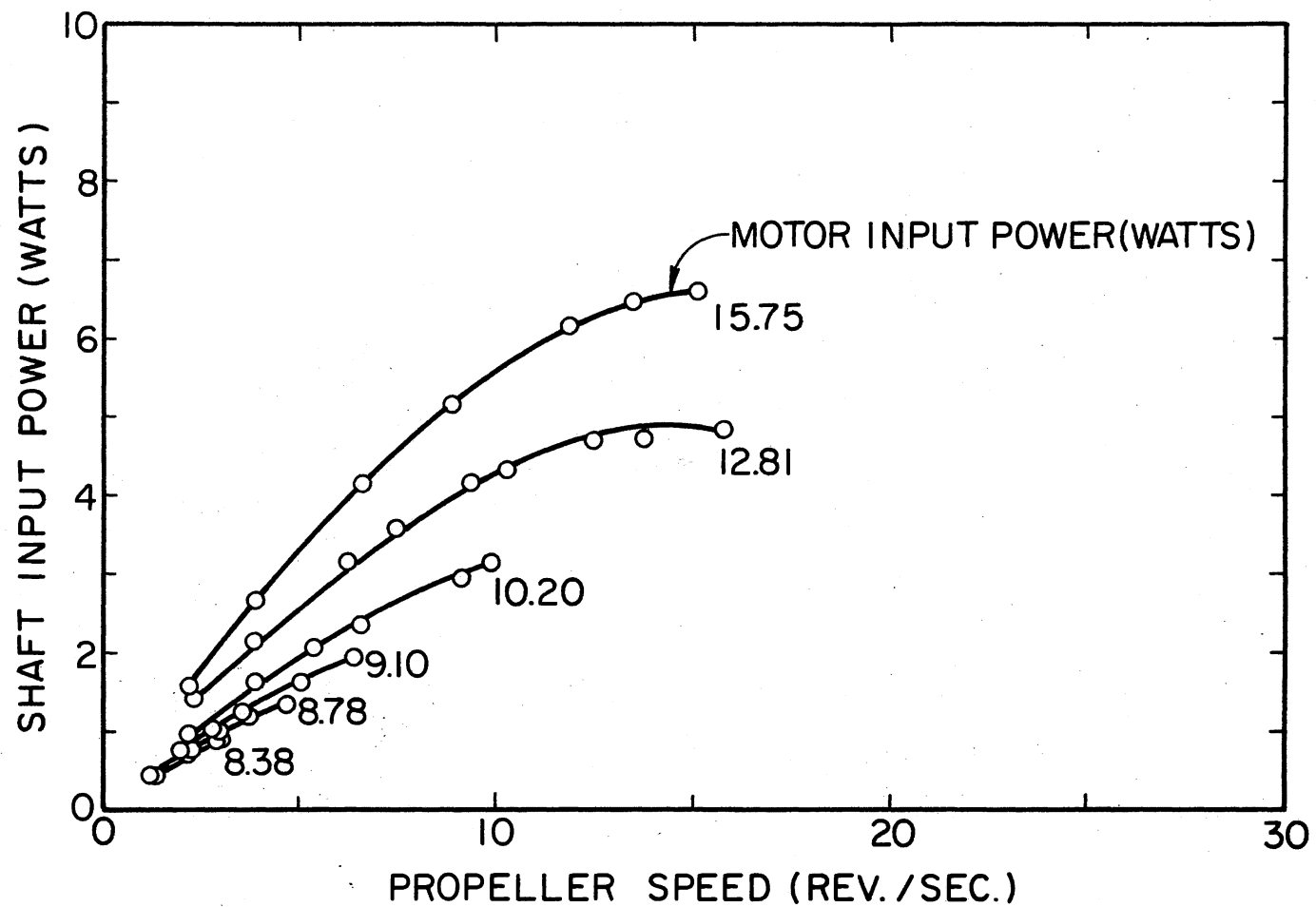


Figure 13. Plot of Shaft Input Power Versus Shaft Rotational Speed for Different Input Powers of the Motor

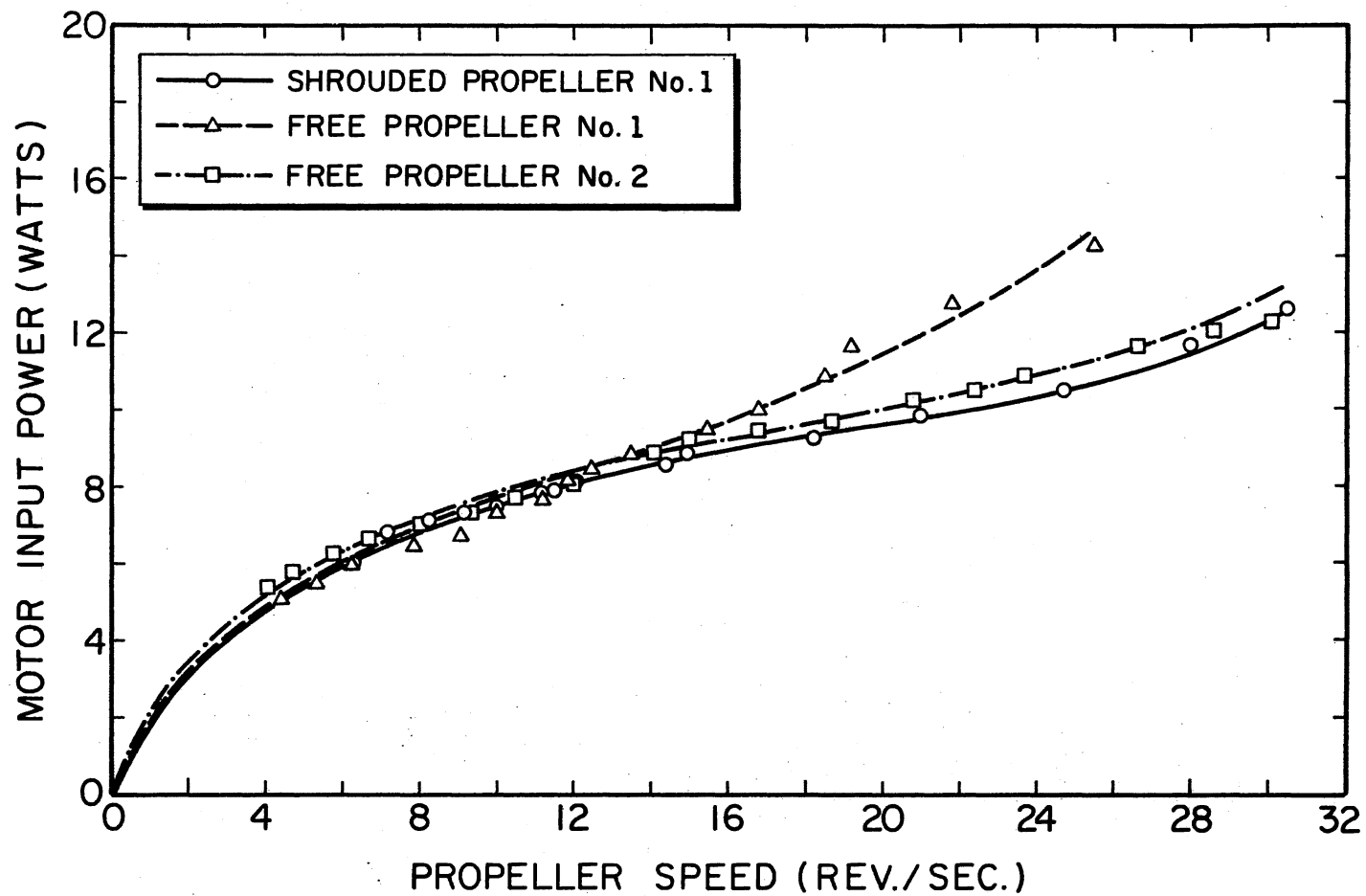


Figure 14. Calibration of Input Power to the Motor Versus Shaft Rotational Speed for Different Configurations

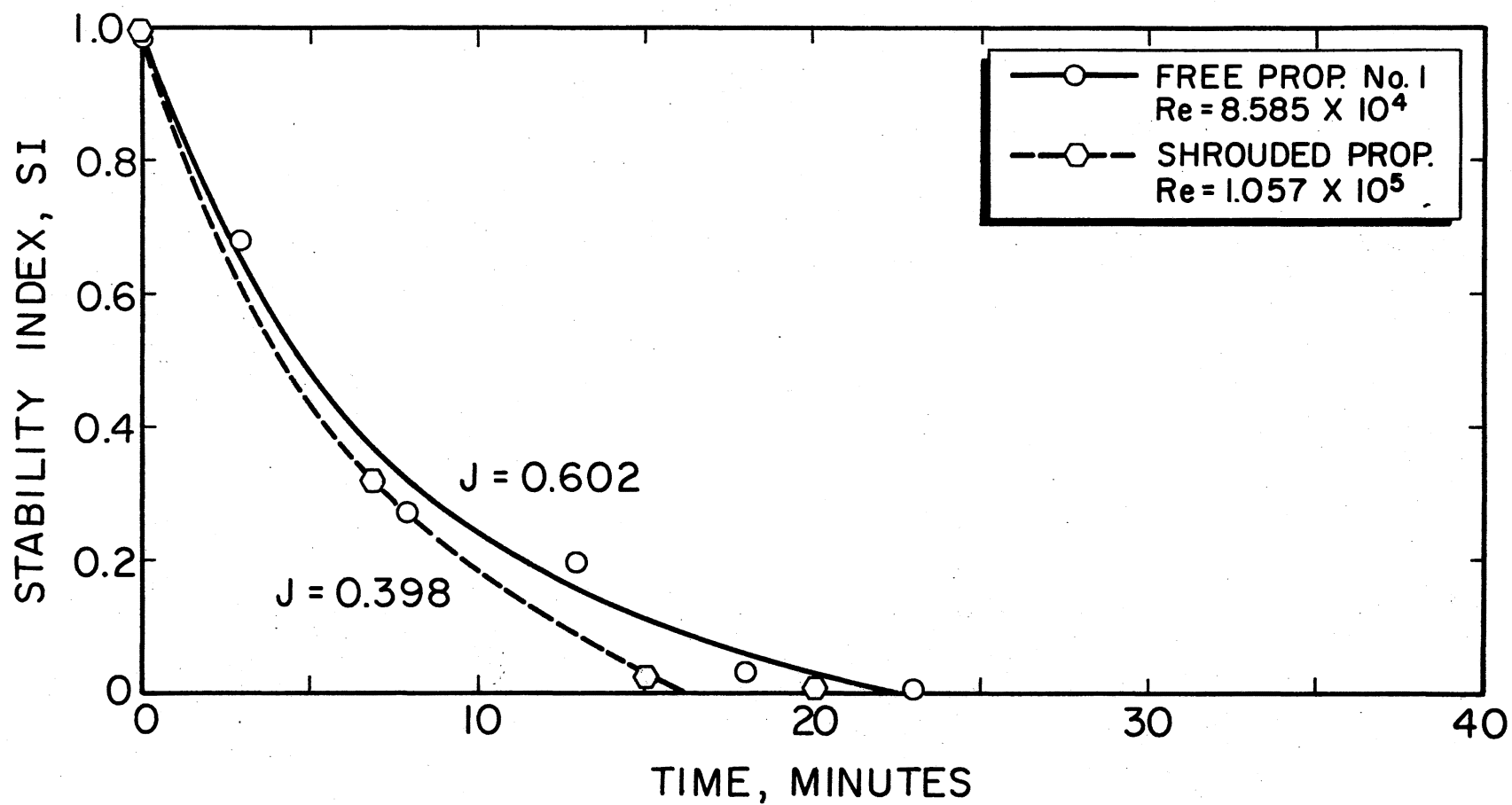
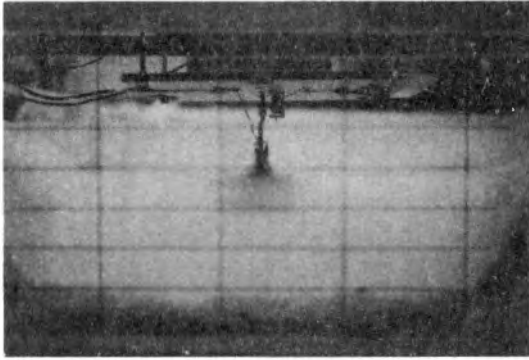
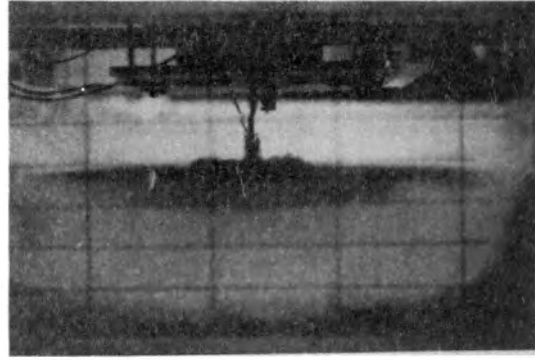


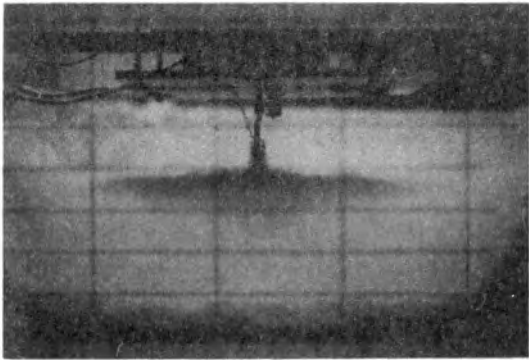
Figure 15. Comparison of Stability Index Measurements Made for Shrouded and Unshrouded Propeller No. 1 With the Same Shaft Input Power



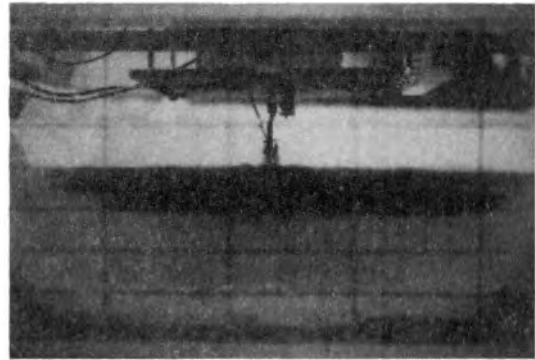
Elapsed time 5 seconds



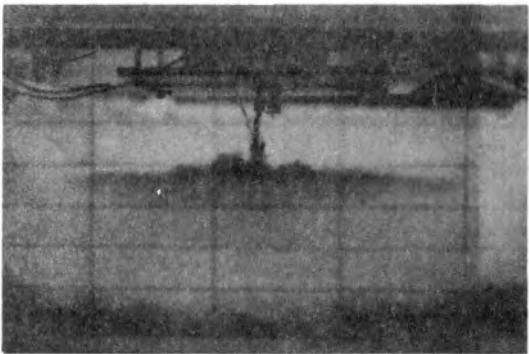
Elapsed time 30 seconds



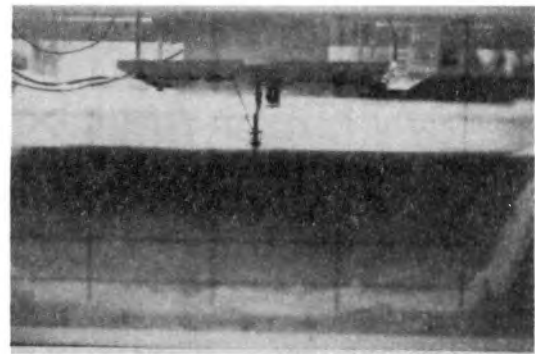
Elapsed time 10 seconds



Elapsed time 50 seconds



Elapsed time 20 seconds



Elapsed time 300 seconds

Figure 16. Visualization of the Lensing Phenomenon
for Free Propeller No. 2

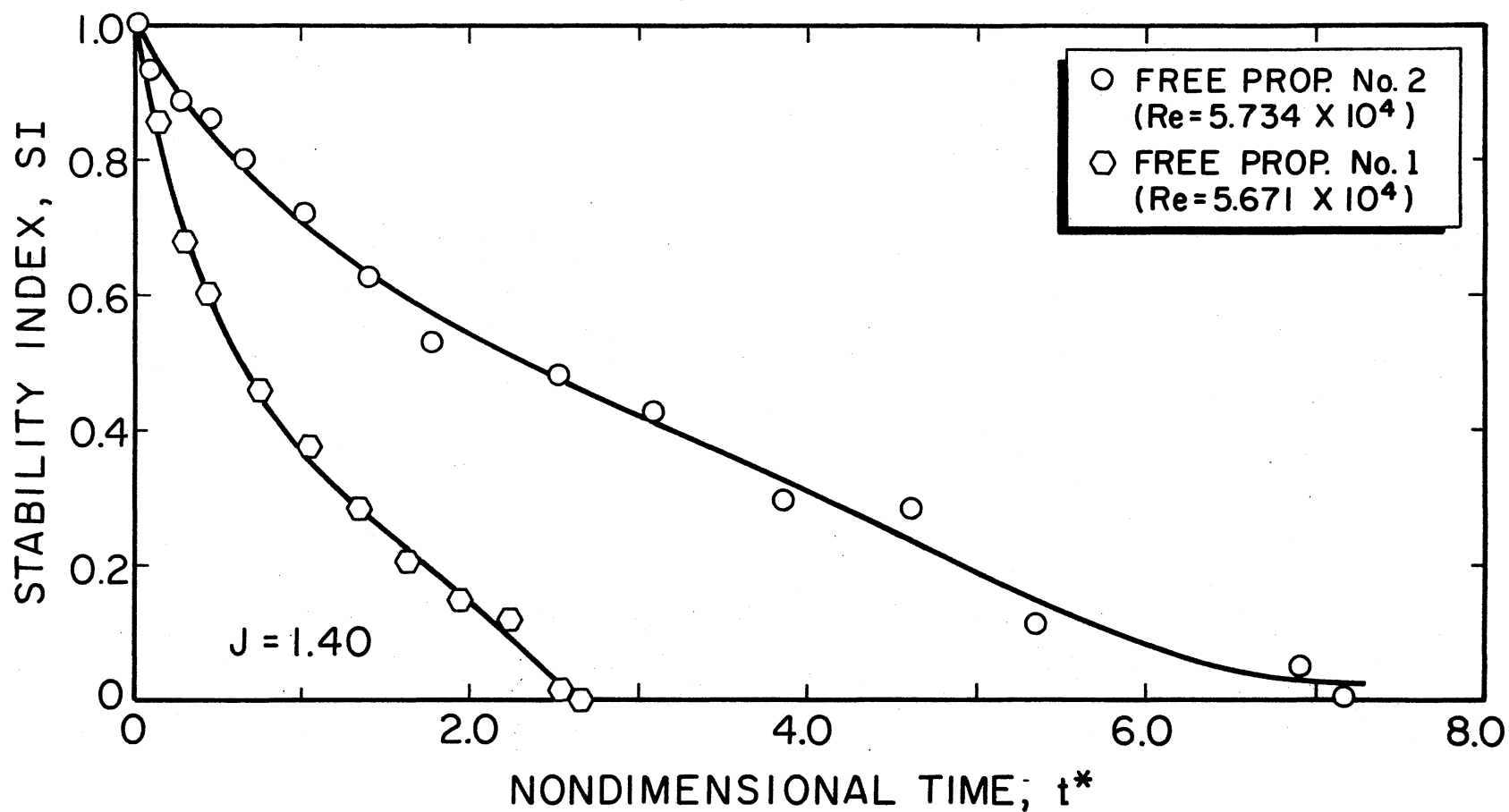


Figure 17. Comparison of Stability Index Measurements Made for Free Propellers 1 and 2 With the Same Richardson Number

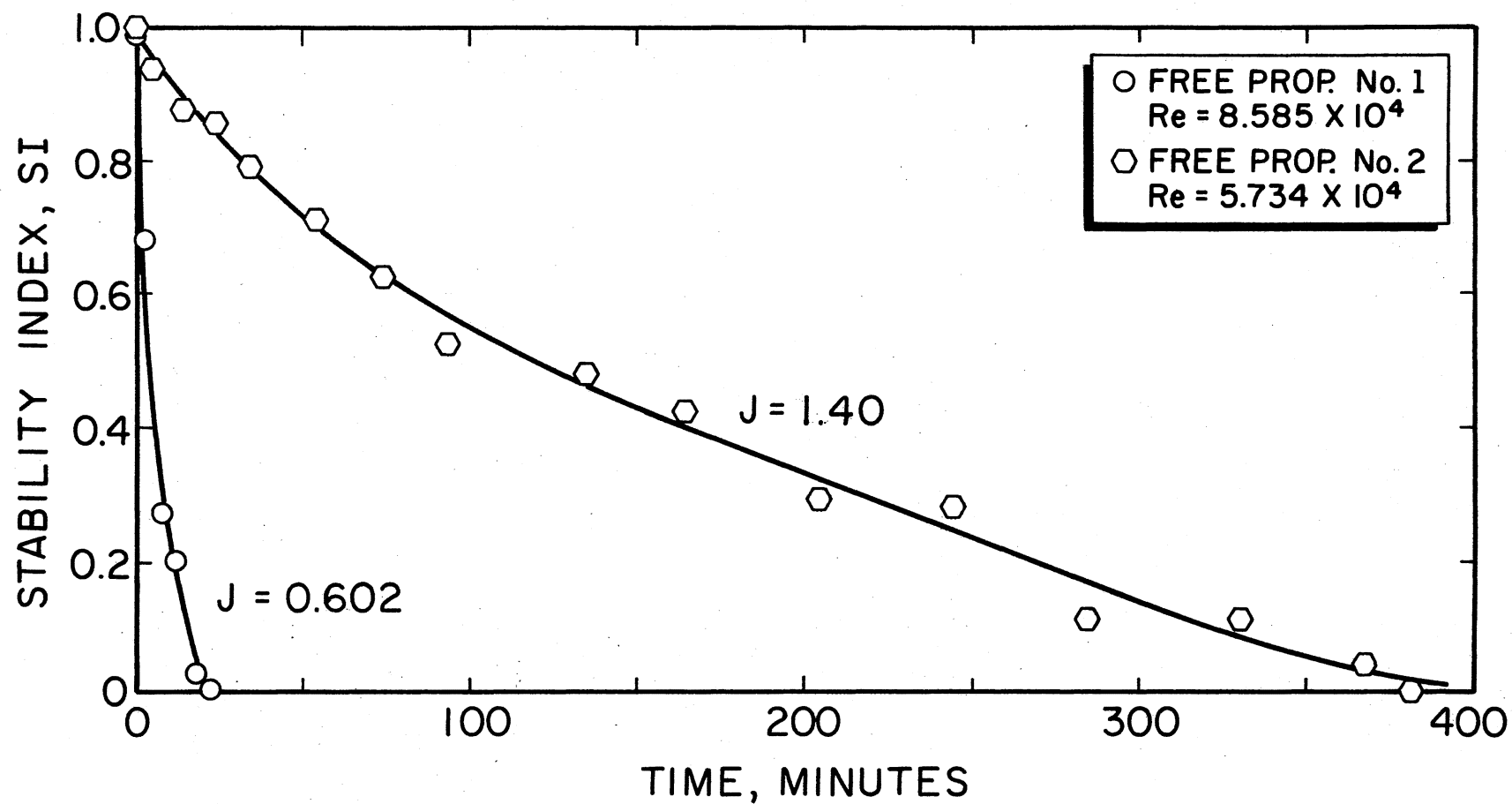


Figure 18. Comparison of Stability Index Measurements Made for Free Propellers 1 and 2 With the Same Shaft Input Powers

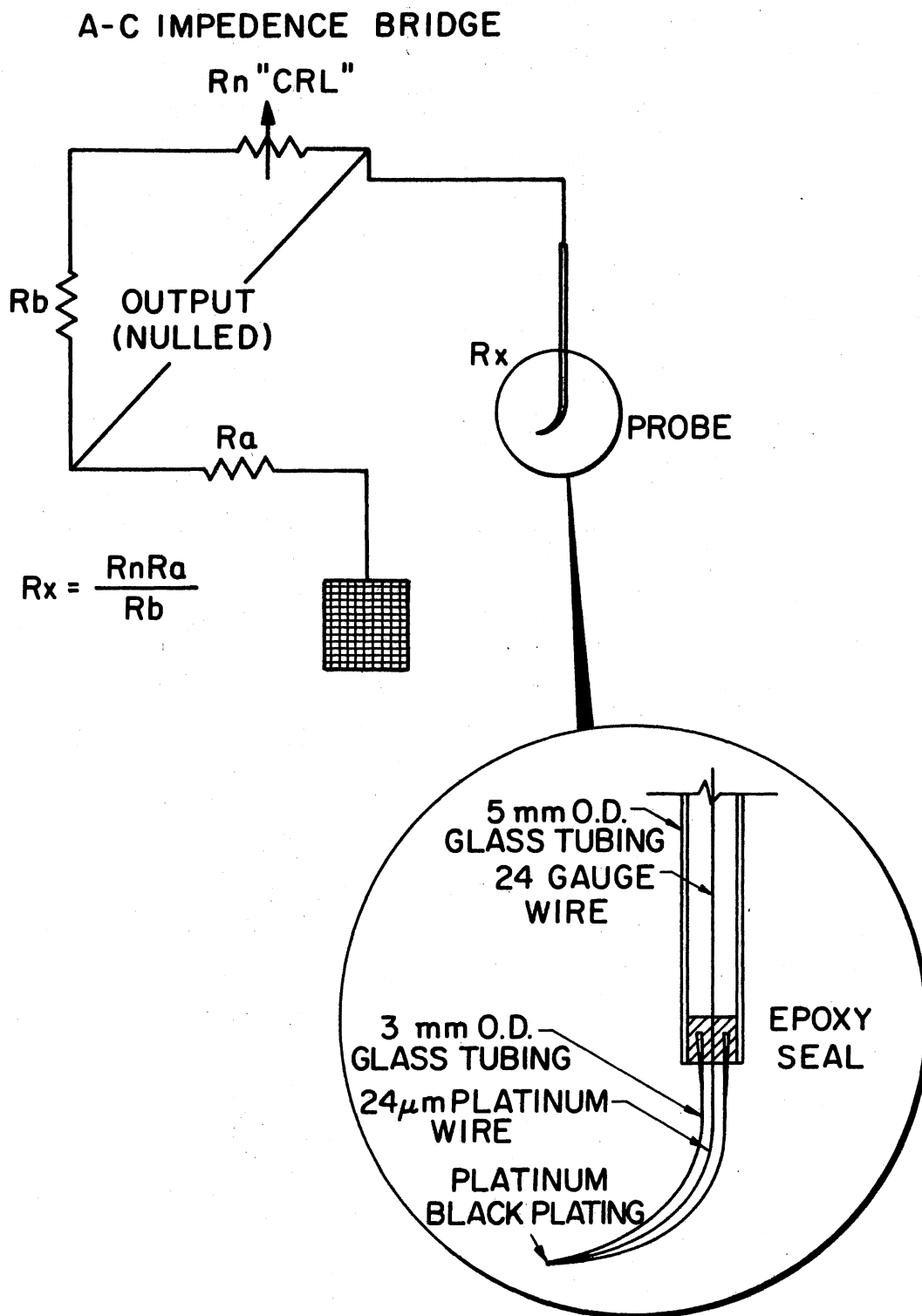


Figure 19. Schematic Diagram of Conductivity Probe

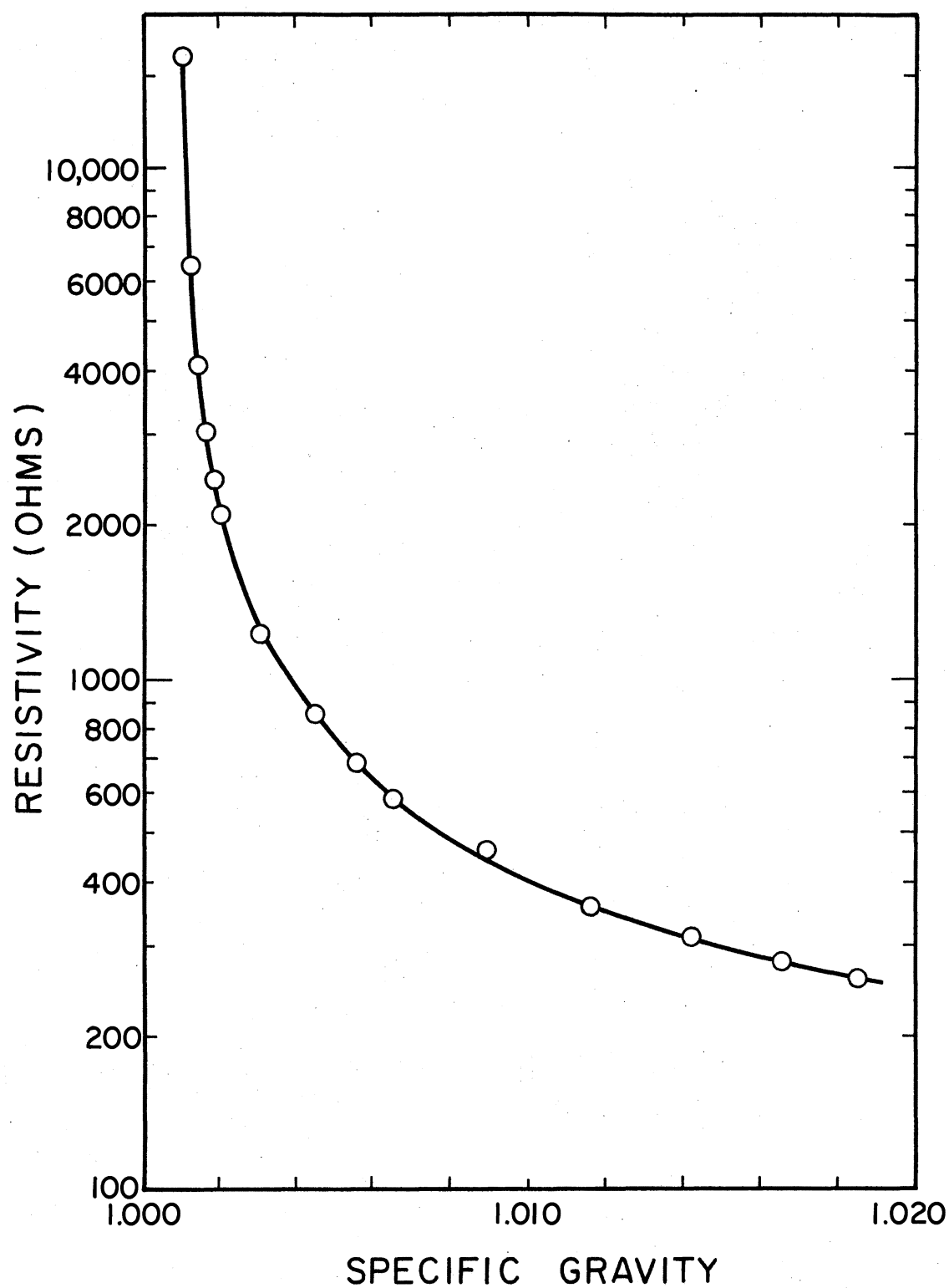


Figure 20. Sample Calibration Curve for a Conductivity Probe

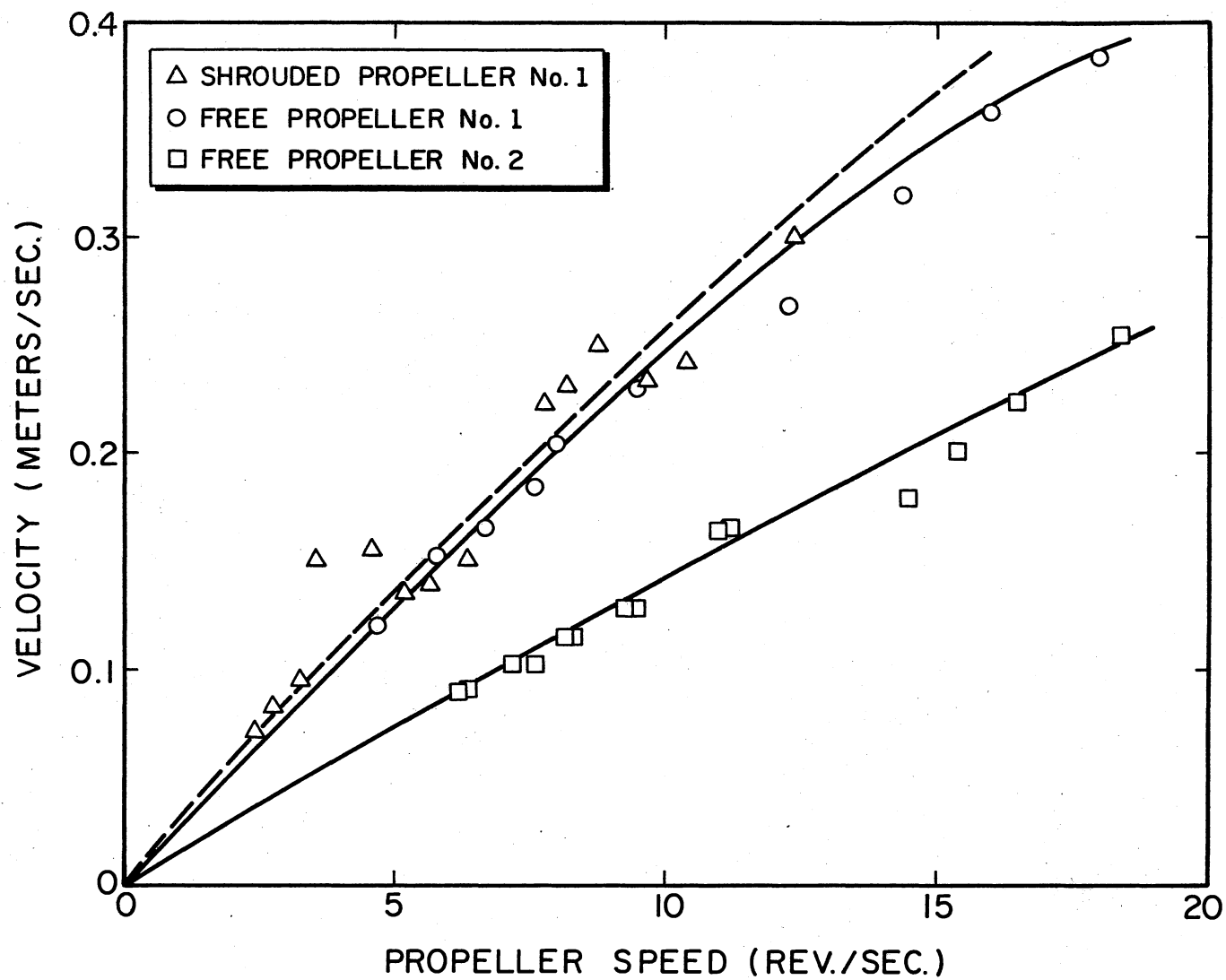


Figure 21. Plot of Velocity Versus Shaft Rotational Speed for Different Configurations

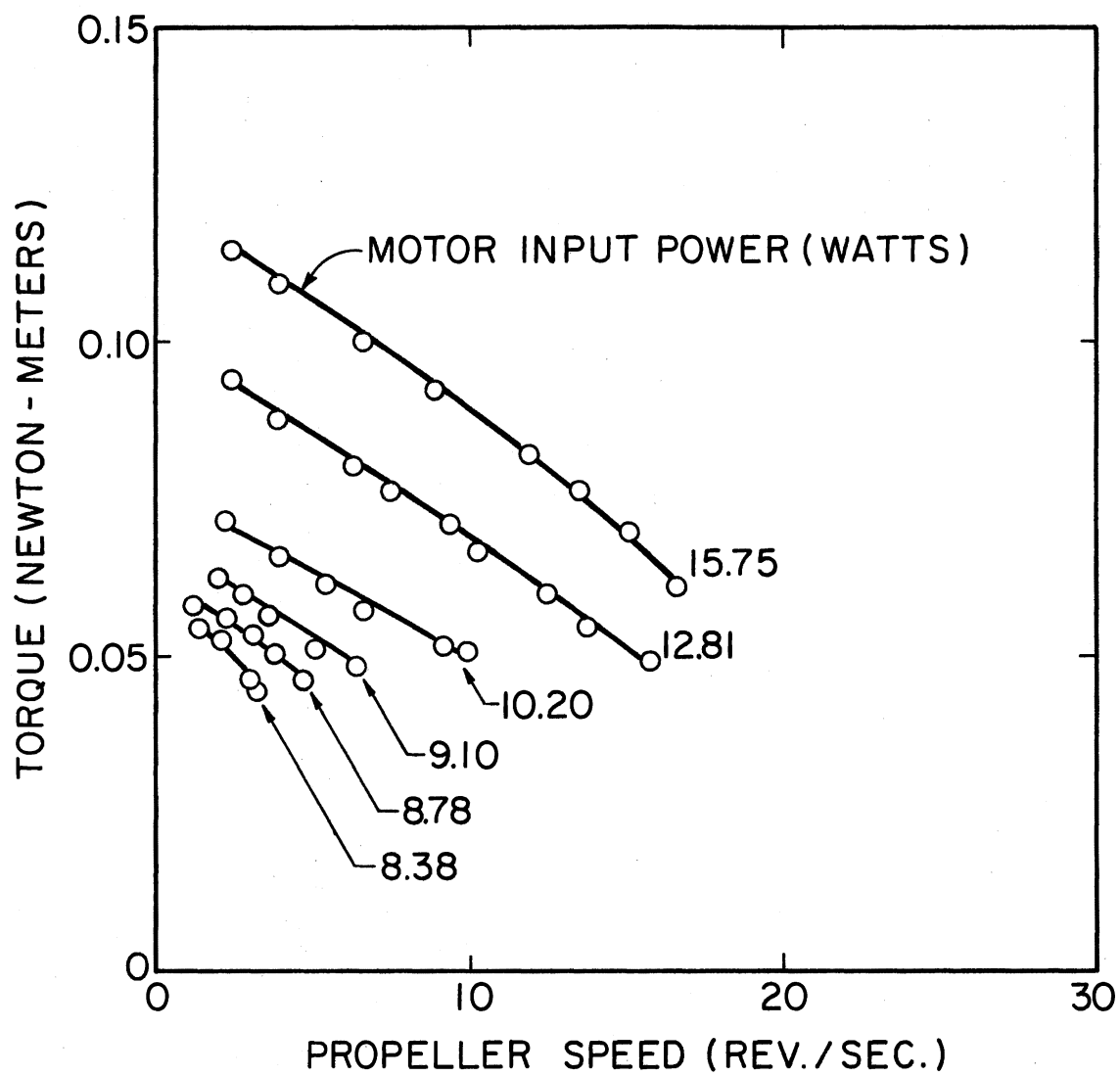


Figure 22. Calibration of Torque Versus Shaft Rotational Speed

APPENDIX B

CONDUCTIVITY PROBE

The method of constructing the conductivity probe proceeds as follows:

First, a 3 mm outside diameter flint glass tube was heated. When the proper temperature was reached, the glass tube was drawn down to an approximate inside diameter of .07 mm. Then a platinum wire of approximately 28 μm in diameter was threaded into the glass tube. The smaller end of this tube was reheated, sealing the platinum wire inside. The tip was carefully shaped with fine sandpaper. The electrolytic solution was made by dissolving 0.3 gram of chloroplatinic acid ($\text{H}_2\text{PtCl}_6\cdot 6\text{H}_2\text{O}$), and .003 gram of lead acetate ($\text{Pb}_{20}(\text{CH}_3\text{COO})_2$) in 10 ml of water. The tip was placed in this solution and standard plating technique was used, and the tip was coated with platinum black. A 5 mm o.d. flint glass tube epoxied to the 3 mm o.d. glass tube provided the main body of the probe. Figure 19 shows the schematic diagram of the probe with the electrical network. The probe tip and a wire mesh screen were used as two electrodes. Immersing these two in the salt water solution completed the circuit of an A-C impedance bridge. Type 1650A impedance bridge was utilized to measure the resistivity of the solution at the probe tip. The resistivity measurements were converted to densities through the calibration curve for the conductivity probe. The conductivity probe was calibrated by measuring the resistivity of several salt solutions over a range of known density. This calibration chart was plotted and is shown in Figure 20. In order to measure a particular density profile in the model, the resistivities were recorded at several different depths. These values were converted to density readings from the calibration curve of density versus resistivity. Then the plot of density versus depth was plotted.

APPENDIX C

VELOCITY MEASUREMENTS

The velocity of the water leaving the propeller was calibrated using a dye tracing technique. A 16 mm Pailard-Bolex high speed movie camera was placed on the side of the model by the dam. Thin strips of black tape were placed on the plexiglass sidewall to serve as markers. The motor was started and the shaft RPM was adjusted to the desired value. The camera was started and the blue dye was injected through a ring-type dye injector placed above the propeller. The dye injector was made out of .32 cm o.d. hypodermic tube. Eight small holes (.5 mm in diameter) were drilled on the ring portion of the injector at approximately the same distances apart and one end of the injector was sealed with the epoxy. The free end of the hypodermic tube was fitted in a tygon tubing and sealed by silicon rubber. The tygon tubing was connected to a dye pot located on the side of the model.

Opening a small valve allowed the dye to enter the water. The movement of the dye leaving the propeller was recorded on film. The shaft RPM was then incremented to a higher value and the same procedure was followed. Several different shaft RPM's were recorded. Data reduction from these recorded films consisted of measuring the distance that the dye front traveled in the duration of five frames. The time during which the dye front traveled this distance was known from the speed setting on the camera. The velocities were calculated by dividing the distance traveled to the time elapsed. The results of this calibration as a function of rotational speed is shown in Figure 21.

APPENDIX D

POWER MEASUREMENTS

Power input to the motor was measured by means of a Hickok digital voltmeter and a Weston ammeter. The product of the voltage and current determined the amount of power input to the motor. The plot of motor input power versus shaft rotational speed for different configurations is shown in Figure 14. The plotted data indicates that the shrouded propeller requires less power input to the motor to drive the system at the same speed as the unshrouded propeller. This phenomenon is more apparent at the higher propeller speeds. However, the efficiency of the motor was changed by varying the propeller speed. An attempt was made to measure the motor efficiencies at different shaft rotational speeds. In order to accomplish this purpose the motor was connected to a 22.6 Newton-meters Lebow torque meter sensor with the electric brakes. A calibrated tachometer was connected to the motor shaft to measure the shaft rotation. The motor was started and the amount of torque produced for different shaft rotational speeds were recorded. The measured torque values were converted to power quantities through the relation

$$\text{Torque} = \text{power into the shaft} \times \text{RPM.}$$

Figure 22 is a plot of measured torques for different values of rotational speed and constant power inputs to the motor. Obtained from this plot is a plot of shaft input power versus shaft rotational speed corresponding to different motor input powers (see Figure 13).

APPENDIX E

COMPUTER PROGRAM

```
0: 1→X
1: ENT "NO OF Y DIV?", R0
2: PRT "THE NO OF"; PRT "DIVISIONS IS",R0
3: ENT "DIV CENT HIGH=R1",R1
4: X+1→X;ENT "NEXT HIGHT",RX;IF R0>X;GTO +0
5: SPC 5;PRT "HIGHTS OF DIV":PRT "CENTERS ABOVE": PRT "BOTTOM"
6: 0→X
7: X+1→X;PRT RX: IF R0>X;GTO +0
8: ENT "RESP VOLUM=R151",R151
9: 151→X
10: X+1→X;ENT "NEXT VOLUME",RX;IF R0>X-150;GTO +0
11: SPC 5;PRT "VOLUMES"
12: 150→X
13: X+1→X;PRT RX;IF R0>X-150;GTO +0
14: 151→X
15: RX→Y
16: X+1→X;RX+Y→Y;IF R0>X-150;FTO +0
17: PRT "TOTAL VOLUME"
18: SPC 2; PRT Y
19: 0→R31
20: SPC 2;ENT "TIME",C1
21: SPC 3;PRT "TIME=",C1
22: ENT "RESP DENS=R101",R101
23: 101→X
24: X+1→X;ENT "NEXT DENS",RX;IF R0>X-100;GTO +0
25: SPC 5;PRT "DENSITIES"
26: 100→X
```

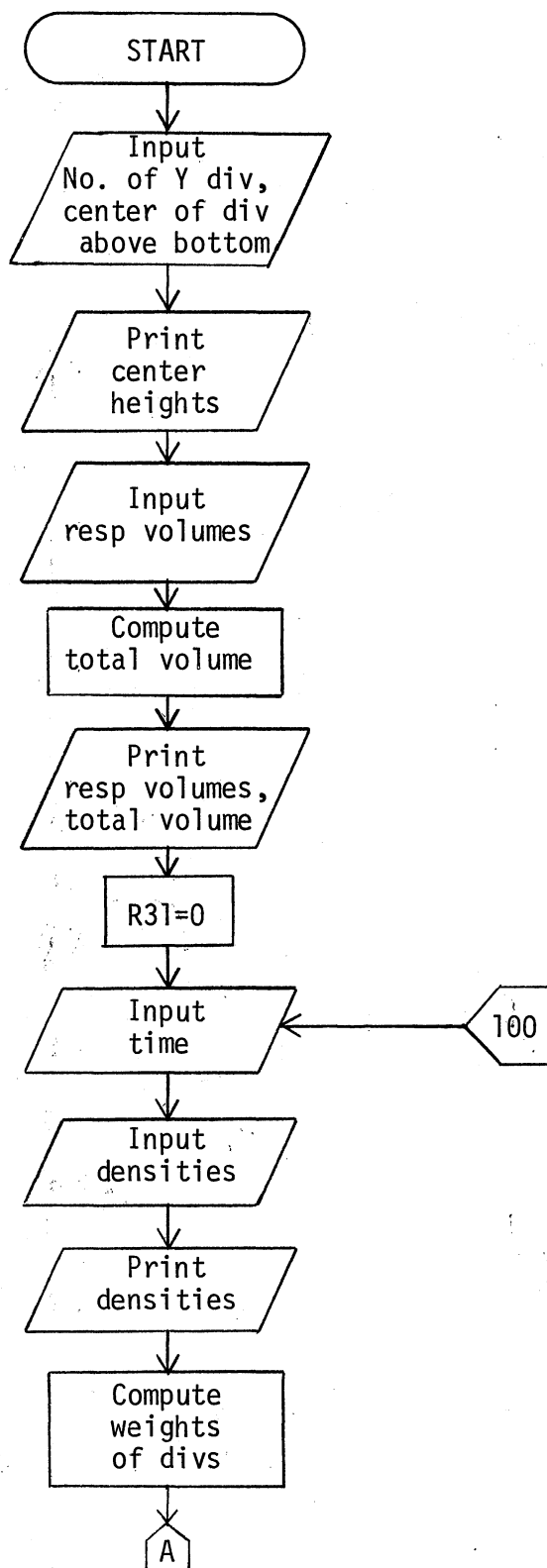
```
27:  X+1→X;PRT RX;IF R0>X-100;GTO +0
28:  100→X
29:  X+1→X;RX*R(X+50)→R(X-50); IF R0>X-100;GTO +0
30:  SPC 5;PRT "WEIGHT OF";PRT "RESPECTIVE";PRT "DIVISIONS"
31:  50→X
32:  X+1→X;PRT RX;IF R0>X-50;FTO +0
33:  51→X
34:  RX→B
35:  X+1→X;RX+B B; IF R0>X-50;GTO +0
36:  IF R31>0;B→R41
37:  R31+1→R31
38:  1→X
39:  RX*R(X+50)→A
40:  X+1→X;RX*R(X+50)+A→A; IF R0>X;GTO +0
41:  A/B→C;SPC 5
42:  PRT "THE CENTER OF";PRT "GRAVITY IS",C;PRT "FT ABOVE BOTTOM"
43:  B/Y→R201;SPC 2
44:  PRT "AVERAGE DENS",R201
45:  C*R41→R202
46:  SPC 5;PRT "P.E. OF";PRT "THE LAKE IS",R202
47:  R202*5.05E-7→R203
48:  SPC 1;PRT "OR";SPC 1;PRT R203;PRT "HP-HRS".
49:  SPC 5;GTO 20
50:  STP
51:  END

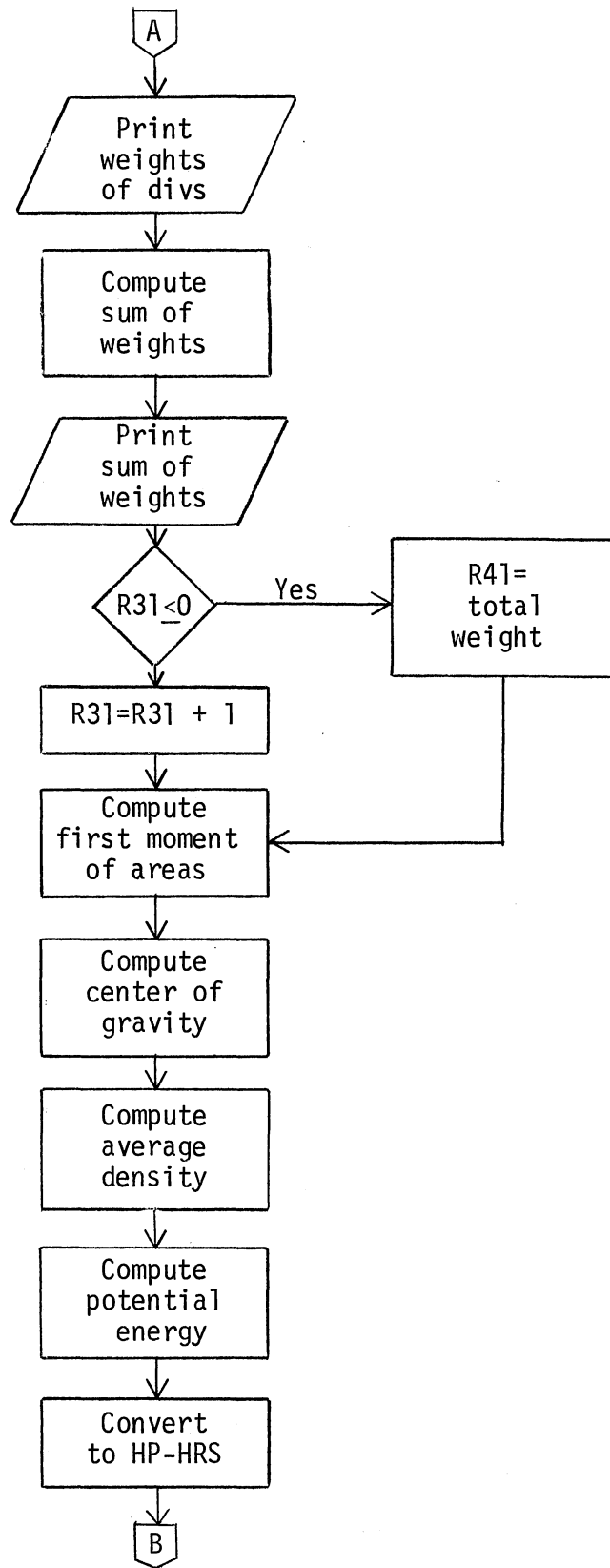
R287
```

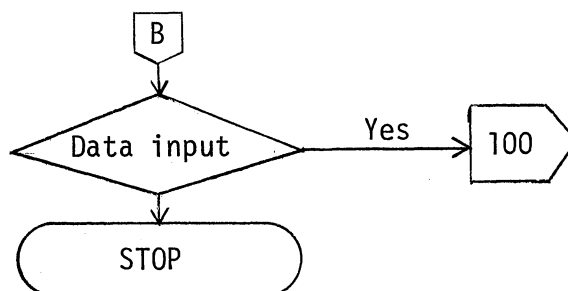
Computer Nomenclature

- A: Sum of all the first moments of areas
- B: Sum of all the weights of the divisions
- C: Center of gravity of the lake above the bottom
- C1: Time at which density profile is recorded
- Y: Total volume of the divisions
- R0: No. of Y divisions
- R1→R10: Center of divisions above bottom
- R31: Logic control variable
- R41: Logic control variable
- R51→R60: Weight of the respective divisions
- R101→R110: Respective densities of the divisions
- R151→R160: Volumes of the divisions
- R201: Average density
- R202: Potential energy of the lake in ft-lbf
- R203: Potential energy of the lake in HP-HRS

Computer Flow Chart







VITA \

Nader Sharabianlou

Candidate for the Degree of

Master of Science

Thesis: HYDRAULIC MODELING OF MECHANICAL DESTRATIFICATION OF LAKES

Major Field: Mechanical Engineering

Biographical:

Personal Data: Born in Tehran, Iran, November 14, 1951, the son of Mr. and Mrs. Rahim Sharabianlou.

Education: Graduated from Ferdowsi High School, Tabriz, Iran, in May, 1969; received Bachelor of Science degree in Mechanical Engineering from Oklahoma State University in May, 1974; completed requirements for Master of Science degree at Oklahoma State University in December, 1975.

Professional Experience: Undergraduate research assistant, Oklahoma State University, 1974; graduate research assistant, School of Mechanical and Aerospace Engineering, Oklahoma State University, 1974, 1976.

Professional and Honorary Societies: American Society of Mechanical Engineers; American Institute of Aeronautics and Astronautics; American Society of Heating, Refrigerating, and Air Conditioning Engineering; Pi Tau Sigma.